

**EBOLA VIRUS INFECTION FOLLOWING A LARGE PARTICLE AEROSOL
EXPOSURE IN NONHUMAN PRIMATES MAY INDICATE A LOW
POTENTIAL FOR HUMAN DROPLET TRANSMISSION**

by

Jordan Kyle Bohannon

Bachelor of Science in Microbiology (Auburn University) 2008

THESIS

Submitted in partial satisfaction of the requirements

for the degree of

MASTER OF SCIENCE

in

BIOMEDICAL SCIENCE

in the

GRADUATE SCHOOL

of

HOOD COLLEGE

May 2020

Accepted:

Ann Boyd, Ph.D.
Committee Member

Ann Boyd, Ph.D.
Director, Biomedical Science Program

Craig Laufer, Ph.D.
Committee Member

Jens Kuhn, M.D., Ph.D., Ph.D., M.S.
Thesis Adviser

April Boulton, Ph.D.
Dean of the Graduate School

STATEMENT OF USE AND COPYRIGHT WAIVER

I do authorize Hood College to lend this thesis, or reproductions of it, in total or in part, at the request of other institutions or individuals for the purpose of scholarly research.

DEDICATION

I dedicate this thesis to my beautiful wife Natalie Bohannon, who has supported and encouraged me throughout my coursework at Hood College.

ACKNOWLEDGEMENTS

Tracey Burdette¹, Matt Lackemeyer¹, Tim Cooper¹, Lisa Mistretta¹, Jonathan Kurtz¹, Ricky Adams¹, Laura Bollinger¹, Reed Johnson², Mike Holbrook¹, Danny Ragland¹, Ian Crozier¹, Phil Sayre¹, Chris Bartos¹, Ji Hyun Lee¹, Peter Jahrling¹, Jens Kuhn¹

1. Integrated Research Facility, National Institutes of Allergy and Infectious Diseases, National Institutes of Health, Frederick, MD, USA

2. Emerging Viral Pathogens Section, National Institute of Allergy and Infectious Diseases, National Institutes of Health, Frederick, MD, USA

This research was performed at the Integrated Research Facility at Fort Detrick (IRF-Frederick), Clinical Monitoring Research Program Directorate, Frederick, National Laboratory for Cancer Research and sponsored by the National Cancer Institute, Frederick, MD, USA

TABLE OF CONTENTS

	Page
ABSTRACT	vii
LIST OF TABLES	viii
LIST OF FIGURES	ix
LIST OF ABBREVIATIONS	x
INTRODUCTION	1
MATERIALS AND METHODS	5
Animals	5
Ethics Statement	5
Virus and Cells	6
Aerosol Exposure	6
Virus Titration	8
Quantitative PCR	9
Clinical Analysis	10
Imaging	10
Necropsy and Histopathology	10
Flow Cytometry	11
Cytokine Response	13
RESULTS	15
Aerobiology	15
Clinical Course of NHPs	18
Imaging	19

Flow Cytometry	23
Cytokine Analysis	28
Hematology/Clinical Chem.	28
Anatomic Pathology	32
DISCUSSION	36
REFERENCES	40
Appendices	43

ABSTRACT

Aerosol particle deposition patterns of inhaled aerosol particles are known to affect the virulence of inhaled bioaerosol pathogens. Small particle (0.5–3 μm) aerosols typically deposit within the alveolar regions of the lungs, whereas large particle ($\geq 12 \mu\text{m}$) aerosols tend to deposit within the nasopharyngeal and tracheobronchial regions of the upper respiratory tract in non-human primates (NHPs). A few studies have evaluated pulmonary disease following small particle Ebola virus (EBOV) aerosol inhalation in rhesus macaques, but characterization of upper respiratory tract infection following large particle EBOV inhalation has not been studied. This study determined lethality and characterization of disease course in rhesus macaques following a large particle EBOV aerosol deposition into the nasopharyngeal region. A secondary objective of the study is to characterize the immune response to large particle aerosol inhalation. Each NHP was monitored for respiratory disease by ^{18}F -Fluorodeoxyglucose positron emission tomography computed tomography imaging. Serial hematology and serology assays were also performed to track disease progression throughout the 28-day study. NHPs exposed to target aerosol doses of 1000–10,000 plaque-forming units of EBOV had the upper respiratory tract as a major site of virus-induced pathology. Other pathology findings were similar to an intramuscular EBOV challenge. However, NHPs exposed to a low dose (100 plaque-forming units) of large particle EBOV aerosol did not have any clinical signs or symptoms of EBOV disease and survived through to the study end. These results demonstrate that particle deposition can indeed alter disease course and can be a starting point in exploring the heterogeneity of EBOV virulence seen in humans. These data are also useful in evaluating possible droplet transmission of EBOV.

LIST OF TABLES

Table		Page
1	Aerosol Dosimetry	16
2	Aerosol Particle Size Distribution	17

LIST OF FIGURES

Figure		Page
1	Mean Time to Death for Large Particle Ebov Challenge	19
2	1000 PFU NHP Image	20
3	10,000 PFU NHP Image	21
4	100 PFU NHP Image	22
5	Total Hematopoietic Cells	23
6	Total B Cells	24
7	Total CD4 Cells	25
8	Total CD8 Cells	25
9	Total NK Cells	26
10	Average Monocyte Counts	29
11	Average Platelet Counts	30
12	Average ALT	31
13	Average AST	31
14	IHC tracheal/bronchial lymph nodes	32
15	IM pathology Comparison	33
16	Lung Pathology	34
17	Eye Pathology	35

LIST OF ABBREVIATIONS

APS	Aerodynamic Particle Sizer
BAL	Bronchoalveolar lavage
CXPV	Cowpox virus
DMEM	Dulbecco's Modified Eagle Medium
EBOV	Ebola virus
EDTA	Ethylenediaminetetraacetic acid
EVD	Ebola virus disease
FBS	Fetal bovine serum
FDG	¹⁸ F-Fluorodeoxyglucose
HI FBS	Heat-inactivated fetal bovine serum
IHC	Immunohistochemical
IM	Intra-muscular
NHP	Non-human primate
NIV	Nipah virus
PCR	Polymerase Chain Reaction
PET/CT	Positron emission tomography–computed tomography
PFU	Plaque forming unit
PID	Post Infection Day

INTRODUCTION

Few epidemiological studies investigating possible EBOV transmission patterns in past Ebola virus disease (EVD) are available. Conclusions made about the routes of transmission are based on relatively limited data sets with some interpretations based on constructions of deceased individuals describing the chains of transmission. Transmission information often obtained from surrogates can inherently create a recall bias that has been observed for most of the available epidemiological studies (Osterholm 2015). Current literature indicates that direct physical contact of infected body fluids as the most likely route of EBOV transmission. EBOV has been cultured from body fluids such as urine, breast milk, saliva, and semen of infected patients. Viral RNA has also been detected through polymerase chain reaction (PCR) in tears, sweat, and stool samples and rectal, conjunctival, vaginal, and skin swabs (Bausch 2007, Formenty 2006, Richards 2000, Rowe 1999, Rodriguez 1999).

Disease transmission can also potentially occur through aerosol particles containing viral pathogens. Traditionally, aerosol secretions have been separated into two distinct categories: small ($<5 \mu\text{m}$) and large droplets ($>5\mu\text{m}$). The size of these infectious aerosol particles can range from $0.05\text{--}500 \mu\text{m}$ and can be generated through the emission of body fluids such as respiratory secretions from coughing, sneezing, talking, and exhalation. These aerosol secretions have a polydisperse particle distribution that can potentially carry infectious viruses (Galton 2011). Infectious aerosols can also be generated outside the respiratory tract from medical procedures or incidents of vomiting or diarrhea.

Aerosol transmission is impacted by particle flight time, distance traveled, and time the particles will remain infectious once generated (Osterholm 2015). Variations in particle size, shape, density, and vehicle material also impact transmission. Ambient temperature and humidity play a key role in infectious aerosol survival (Hinds 1999). Results from a previous study has demonstrated that that EBOV can survive in aerosol particles for approximately 100 min (at 50% to 55% relative humidity and $22 \pm 3^{\circ}\text{C}$) (Piercy 2010).

The role of EBOV aerosol transmission in propagation of disease, however, remains unclear. Infectious aerosols (small or large droplets) can transmit disease, including EBOV infection. A study involving intramuscular EBOV inoculated rhesus macaques and uninoculated controls housed in the same room (approximately 3 m away) suggest that the uninoculated control NHPs became infected through the aerosol, oral, or conjunctival exposure to virus-laden aerosol particles. Two of the three control NHPs developed EBOV disease 10 and 11 days after the EBOV inoculated animals had died. Pulmonary antigen staining from pathology specimens suggests that the control NHPs were infected via aerosol particles. (Jaax 1995).

Well characterized inhalational animal disease models are often required to develop medical countermeasures in lieu of human efficacy data (Food and Drug Administration, 2014b, Food and Drug Administration, 2014a). NHPs are commonly chosen as the standard animal model because they are more closely genetically related to

humans than laboratory animals of other species. NHPs tend to share a common aerosol particle deposition pattern in their respiratory tract that is comparable to humans. (Cheng 2008, Raabe 1988, Dabisch 2017).

Most investigators studying NHP aerosol models use small, monodisperse pathogen-containing aerosol particles ranging from 1–3 μm in diameter (May 1966, Reed 2011, Barnewall 2012, Reed 2005, Alves 2010, Hartman 2014, Nalca 2010, Lee 2013, Zumbun 2012, Yeager et al., 2012). Limited data sets are available that compare viral aerosol deposition patterns in NHPs. Johnson proved that the lethality of cowpox virus (CPXV) is a function of particle size in NHPs (Johnson 2014). Lee developed a large particle Nipah virus (NIV) aerosol (approximately 12- μm) model in African green monkeys (Lee 2019). This study also proved the importance of particle size in regards to NIV disease lethality and disease course. Four of 6 animals exposed to large particle NIV showed abnormalities reminiscent to that of human disease. From previous studies evaluating the disease course following a small particle EBOV aerosol exposure in NHPs (Reed 2011, Twenhafel 2013), a severe pulmonary disease developed in rhesus macaques that was uniformly lethal at 1000 plaque forming units (PFU).

To our knowledge, no one has investigated a large particle EBOV aerosol exposure in rhesus macaques. This study was designed to target the upper respiratory tract in rhesus macaques with large particle (10–14 μm) aerosols to mimic an aerosol droplet exposure. The objective of the study was to monitor and characterize the disease course. A large particle aerosol inoculation approach to study NHP EBOV infection and

to control the site of particle deposition may play a key role in understanding disease presentation and disease course and immune responses to EBOV infection.

MATERIALS AND METHODS

Animals

Fourteen male and four female rhesus macaques (*Macaca mulatta*) were used in the study as test subjects. The NHPs were singly housed prior to and after assignment to the study and were provided appropriate enrichment, including, polished steel mirrors and durable toys. All NHPs were anesthetized in accordance with biosafety level-4 standards prior to all procedures including large particle aerosol challenge, positron emission tomography/computerized tomography (PET/CT) imaging, and blood collection. NHPs were monitored following anesthesia to ensure recovery.

Euthanasia criteria were based on a 4-point scoring system that accounted for clinical signs/symptoms of disease (e.g., lethargy, inappetence, weight loss, skin rash, respiratory distress). Secondary criteria, such as platelet counts and blood chemistry, were also evaluated for euthanasia decisions based on veterinary discretion.

Ethics statement

Work with NHPs was conducted in accordance with an Animal Study Protocol approved by the National Institute of Allergy and Infectious Diseases (NIAID) Division of Clinical Research, Animal Care and Use Committee following recommendations in the Guide for the Care and Use of Laboratory Animals. This institution also accepts as mandatory the Public Health Service policy on Humane Care and Use of Laboratory Animals. All NHP work at NIAID was performed in a facility accredited by the Association for the Assessment and Accreditation of Laboratory Animal Care International.

Virus and cells

The study used the Makona isolate of EBOV (Ebola virus/*H.sapiens*-tc/GIN/2014/Makona-C05). The stock was propagated from the passage 2 (p2) of Ebola virus Makona-C05 Master stock (BioSample SAMN04488486, IRF0136_EBOV) in VERO C1008 (E6) cells (African green monkey kidney cells, Working Cell Bank, NR-596 obtained through BEI Resources, (NIAID), National Institutes of Health (NIH), Manassas, VA). Virus stock was propagated using Minimum Essential Medium-alpha, GlutaMAX, no nucleosides (Gibco, ThermoFisher Scientific) supplemented with 2% US-origin, certified, heat-inactivated fetal bovine serum (HI-FBS, Gibco, ThermoFisher Scientific). Following harvest, HI-FBS was diluted to 10% final concentration prior to virus cryopreservation.

For the large particle EBOV aerosol exposures, challenge material was thawed, pooled, diluted prior to aerosol challenge, and kept on ice. EBOV stock was serially diluted into Dulbecco's Modified Eagle Medium (DMEM) (Lonza, Walkersville, MD) supplemented with 2% heat inactivated FBS) and 15% glycerol (Sigma–Aldrich, St. Louis, MO).

Aerosol exposure

Three groups of NHPs (n = 18) were exposed to a large particle EBOV dose based on group assignment. NHPs were randomly assigned to dose groups: EBOV target doses in Groups 1–3 were 100 PFU, 1,000 PFU, and 10,000 PFU, respectively. NHPs were exposed to large particle EBOV ($12.95 \pm 0.74 \mu\text{m}$) aerosol using a 16 liter, head-only, aerosol exposure chamber. The 3 groups of NHPs were exposed on separate days to

accommodate imaging procedures (PET/CT) associated with the study. An aerosol management platform (AeroMP, Biaera Technologies, USA) within a Class III biosafety cabinet (Germfree, FL, USA) was used to conduct the aerosol challenge. The AeroMP attaches to a dedicated house air supply and vacuum ports and controls parameters that influence aerosol delivery, such as temperature and humidity of the air and input airflow to each device attached to the AeroMP. Negative pressure (-0.1" WC) was maintained in the aerosol head-only chamber by AeroMP and in the Class III biosafety cabinet by double high efficiency particulate air-filtered exhaust systems throughout each experiment.

NHPs were anesthetized with ketamine (10 mg/kg, IM) and tiletamine and zolazepam in fixed combination (4–6 mg/kg, IM) and received a single, time-calculated aerosol challenge dose. Respiration parameters at steady state were measured using a calibrated pneumotachograph mask placed over the NHP's snout prior to the aerosol exposure (Data Sciences International, Brighton, MN) using Ponemah software) (Besch 1996). The viral suspension was loaded into a 60-ml syringe and placed in a syringe pump to feed fresh virus suspension into the centered flow tangential aerosol generator (CenTAG) at a rate of 1 ml/min. CenTAG received input air from 2 passive high efficiency particulate air filters upstream of the aerosol generator and 12 L/min dilution air from the AeroMP. Large aerosol particles (10–14 μm) were generated by CenTAG (CH Technologies, NJ, USA). A 25-l/min siphon vacuum was also used during CenTAG operation to syphon off smaller satellite aerosol particles during aerosol generation. Large particles were used to target the tracheobronchial/nasopharyngeal regions of the NHP

respiratory tract. An aerodynamic particle-sizer (APS) device (TSI, Shoreview, MN, USA) measured particle size in real-time for each exposure.

Virus aerosol concentrations were obtained by an aerosol sampler consisting of a 47-mm gelatin filter (Sartorius 12602-47-ALK filter, Stedim Biotech, Germany) within a stainless-steel filter holder (In-Tox Products, Albuquerque, NM) near the breathing zone of the NHP. The filter receives air from a vacuum from AeroMP at a continuous flow rate of 2 l/min. Each gelatin filter was dissolved in DMEM supplemented with 2% FBS to culture virus collected and calculate the EBOV aerosol concentration (PFU) of the head-only exposure chamber for each NHP. An estimated inhaled dose was calculated using the simplified formula $D = R \times C_{aero} \times T_{exp}$, in which D is the estimated inhaled dose (PFU), R is the respiratory minute volume (L/min), C_{aero} is the aerosol concentration (PFU/L), and T_{exp} is the duration of the exposure (min). A 5-min air wash of the head-only exposure chamber was performed between each NHP challenge to allow the previously generated particles to decay within the head-only chamber.

Virus titration

Viral load of NHP tissue (10% homogenate), liquid, and aerosol filter samples were determined by a plaque assay. VeroE6 cells were plated into a 6-well plate the day before assays were completed for a confluency of 90%–100%. Cells were maintained in DMEM (Gibco) with 10% HI FBS (Sigma). Ten-fold serial dilutions were made of each sample in DMEM (Gibco) with 5% HI-FBS (Sigma) and 5% Antibiotic-Antimycotic (Gibco). Media were aspirated from each well, and 300 μ l of diluted sample were added to the confluent cells and analyzed in triplicate. Plates were incubated for 1 hr at 37°C

with 5% CO₂ and gently rocked every 15 min. A 1:1 mix of 2X Modified Eagle Medium (MEM) (Gibco) with 10% HI FBS, 10% Antibiotic-Antimycotic (Gibco), and 10% GlutaMAX (Gibco) and 2 .5% Avicel RC 591 were overlaid on the monolayers and incubated for 8 days at 37°C with 5% CO₂. After incubation, the overlay was removed, and the cells were fixed in 10% neutral buffered formalin (ThermoScientific) and stained with 0.2% Crystal Violet (Ricca Chemical) for 30 min. After 30 min, the stain was removed, plates were rinsed in water, and the plaques were then counted.

Quantitative polymerase chain reaction

Quantitative polymerase chain reaction (qPCR) was also performed on K3-ethylenediaminetetraacetic acid (EDTA) plasma, nasopharyngeal swabs, cerebrospinal fluid (CSF), and eye fluids and tissues. All samples were inactivated in TRIzol LS (ThermoFisher Scientific). RNA was isolated using the QIAmp Viral RNA Mini Kit (QIAGEN), following the manufacturer's protocol. Briefly, 70 µl of the TRIzol-inactivated sample was added to 280 µl of QIAGEN Buffer AVL containing carrier RNA and internal control. The sample was eluted in 70 µl of QIAGEN Buffer AVE, divided into 2 equal aliquots, and frozen until the assay is performed. Each sample's viral load was measured on an ABI 7500 FastDx real-time PCR instrument (Applied Biosystems, ThermoFisher Scientific) using the BEI Resources Critical Reagents Program (CRP) EZ1 qRT-PCR assay kit, following the manufacturer's instructions. A synthetic RNA standard curve was used, and samples were reported as viral RNA copies/ml of sample.

Clinical analyses

Complete blood counts with a five-part differential and reticulocytes were measured on the Sysmex XT2000iV automated hematology analyzer (Sysmex). Serum chemistries were measured on the Abaxis Piccolo using the General Chemistry 13 standardized analysis panel (Abaxis).

Imaging

NHPs were imaged once prior to study start to establish baseline images and then on study scheduled day post-exposure. 18F-fluorodeoxyglucose (18F-FDG; PN: UD-3003001; Cardinal Health, Beltsville, MD) was injected into the NHPs prior to PET/CT imaging (Phillips).

Necropsy and histopathology

All macaques were humanely euthanatized in accordance with predefined experimental endpoints, and gross necropsy was performed by an American College of Veterinary Pathologists diplomate. Selected tissues, including samples of upper and lower respiratory tract, were collected and fixed in 10% neutral buffered formalin. The nasal cavity was cut into transverse (cross) sections with a Stryker saw (Mopec, Oak Park, MI), followed by decalcification with Immunocal (StatLab, McKinney, TX). Methods for histology and EBOV immunohistochemistry have been previously described (Perry 2018). Selected tissues were immunostained for mouse anti-EBOV matrix protein (VP40) antibody (1:1500; 3G5, catalog 0201-016; IBT Bioservices, Rockville, MD) or rabbit anti-EBOV glycoprotein (GP) antibody (1:14,000; catalog 0301-015; IBT Bioservices). All tissues other than eyes were visualized with 3, 3'-diaminobenzidine

(DAB, brown) chromagen with hematoxylin (blue) counterstain. Because of the native brown melanin pigment in the uveal tract, eyes were stained with Warp Red chromagen (Biocare Medical) with hematoxylin and eosin counterstain.

To detect EBOV RNA in formalin-fixed, paraffin-embedded (FFPE) tissues, in situ hybridization (ISH) was performed using the RNAscope 2.5 HD RED kit (Advanced Cell Diagnostics, Newark, CA, USA) according to the manufacturer's instructions. Briefly, 20 ZZ probe pairs targeting the genomic EBOV VP40 gene were designed and synthesized by Advanced Cell Diagnostics (catalogue 507141). Signal hybridization was visualized with red chromogen and hematoxylin and eosin counterstain. Detailed ISH methods were previously published (Cooper 2018).

Flow Cytometry

Whole blood was collected from each NHP at baseline (day -5), at postinhalation day (PID) 3, 5, 7, and at necropsy. Blood was collected in K3-EDTA vacutainer tubes, before dividing into aliquots and storage at 4°C until processing for flow analysis. Whole blood (100 µl) was first blocked with 5 µl of Human TruStain FcX Solution (BioLegend) on ice for 10 min. Surface stain antibody cocktail (100 µl) was added to the solution and incubated on ice for 20 min (see table below for panel) . Red blood cells (RBCs) were lysed by 1 ml of 1X FACS Lysing solution (BD Bioscience) and incubated at room temperature for 10 min. Samples were centrifuged at room temperature for 5 min at 500 g, washed with 1X annexin V binding Buffer (BD Bioscience), and fixed and permeabilized with 500 µl of Fixation/Permeabilization Buffer (BD Bioscience) at room temperature for 30 min. Processed lysed RBCs were centrifuged at room temperature for

5 min at 550 g and then washed with 1X Perm Wash (BD Bioscience). Such lysates were stained intracellularly with 100 µl of antibody cocktail in 1X Perm Wash for 30 min at room temperature, washed with 4 ml of 1X Perm Wash, and centrifuged at 550 g for 5 min. PBS was used to re-suspend samples and kept at 4°C in the dark until acquisition on a four-laser LSRT Fortessa cytometer (BD Bioscience).

Lung and bronchial alveolar lavage (BAL) samples were collected from each NHP at necropsy and processed into single cell suspensions. The lung collected by the Integrated Research Facility (IRF) Pathology team was placed into a 50-ml conical tube containing 10 ml of Roswell Park Memorial Institute + 10% FBS (RPMI-10) media and transferred to the Immunology Team. Each sample was dissociated using the gentleMACS Dissociator (Miltenyi Biotec) by placing approximately 500 mg of lung tissue into a C-tube containing 5 ml of dissociation cocktail. This cocktail consisted of 4.9 ml of sterile 4-(2-hydroxyethyl)-1-piperazineethanesulfonic acid (HEPES) buffer with 100 µl of collagenase D (100 mg/ml) and 40 µl of DNase I (10,000 U/ml) (Sigma). The sample was homogenized using gentleMACS lung program 37c_m_LDK_1 at 37°C for approximately 45 min. At the end of processing, the sample was spun at 500 g for 5 min at room temperature to remove any cells or tissue from the cap of the C-tube. Samples were resuspended and filtered with a 100-µm filter. The cells were washed with PBS + 2% FBS + 2 mM of EDTA, and RBCs were lysed by the addition of ACK Lysis Buffer for 3–5 min (Quality Biologics). After lysis, an additional wash step was performed prior to cell counting. For each sample, 5–10 x 10⁶ cells were transferred to a flow tube and subsequently stained as described above.

For BAL samples, Comparative Medicine IRF staff lavaged the right and left side of the lungs with 40 ml of PBS using a bronchoscope. The lavage effluent was collected into a 50-ml conical tube and transferred to the Immunology Team. Each BAL sample was centrifuged at 500 g for 5 min at room temperature. If appreciable amounts of RBCs were present, the samples were ACK lysed as described above. If RBCs were minimal in BAL samples, the samples were counted, and 5×10^6 cells were transferred to a flow tube for subsequent staining as described above.

Cytokine response

Plasma from the EBOV-exposed NHPs were tested for cytokine secretion with the MILLIPLEX MAP Non-Human Primate Cytokine Magnetic Bead Panel - Premixed 23 Plex following manufacturer's instructions (Millipore Cat. No. PCYTMG-40K-PX23). All reagents were warmed to room temperature. Quality controls and standards were reconstituted with 250 μ l of deionized water that settled for 10 min prior to use. A seven-point standard curve was generated by diluting the concentrated stock four-fold with assay buffer for each point. The blank was the assay buffer alone. To begin, the plate was first washed with 200 μ l of assay buffer and incubated on an orbital shaker at room temperature for 10 min. The assay buffer was decanted, and the plates were inverted on absorbent paper to remove any excess buffer. To wells denoted for background, controls, or standards, 25 μ l of serum matrix were added. To the sample wells, 25 μ l of assay buffer were added. To the appropriate wells, 25 μ l of samples, standards, or controls were added. The premixed beads were vortexed to resuspend them, and 25 μ l of the beads were added to each well. Each plate was sealed with a plate sealer, and the plates were incubated overnight at 4°C on an orbital shaker.

After overnight incubation, the plates were washed twice using a hand-held magnetic plate holder with 200 μ l of wash buffer per well and decanted as previously described. The plates were then incubated at room temperature for 1 hr with 25 μ l of detection antibody. After incubation, 25 μ l of streptavidin-phycoerythrin were added directly to each well and incubated at room temperature with agitation for 30 min. The plates were washed twice, and 150 μ l of sheath fluid were added to each well. The plates were read on the Flexmap 3D reader (Luminex) per assay instructions within 24 hr of completion.

The data were exported to Bio-Results Generator 3.0 and Bio-Plex Manager (Bioplex). Results were graphed using Prism (GraphPad). For graphing purposes, animals were divided in to three groups: Exposed/Uninfected group, 1,000 PFU exposure group and 10,000 PFU exposure group. Data were graphed per analyte across the three groups, showing the mean concentration of each analyte (pg/ml) and the standard error of measurement for the group. The lower limit of quantification was also included on each graph, as determined per each analyte's standard curve. Individual graphs for each analyte for each NHP were also generated.

RESULTS

Aerobiology

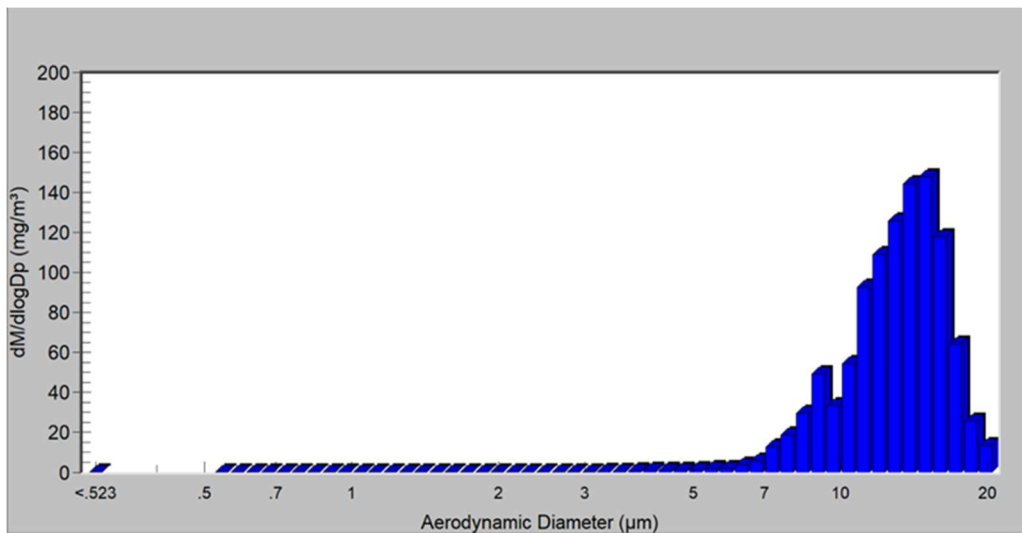
Aerosol estimated inhaled dose for each individual NHP is found in **Table 1**. An inhaled dose was not calculated for NHP 11 due to a malfunction with the aerosol large particle generator. This NHP is believed to have been exposed to small particles in addition to large particles. The pathology and time to death also support this hypothesis for this NHP (NHP 11). During each NHP exposure, a particle size sample was collected to monitor particle size and distribution. Aerosol particle size was reported in aerodynamic diameter along with their respective geometric standard deviations (**Table 2**).

Table 1: Group designations of rhesus macaques challenged with EBOV. Aerosol estimated inhaled dose for each individual NHP.

100 PFU Dose Group 1					
NHP ID	Aerosol Concentration (PFU/ ml)	Minute Volume (L)	Time (min)	Aerosol Volume (L)	Actual Dose (PFU)
1	1.30E+01	2.8	7	19.6	254.1
2	1.26E+01	1.9	10	19	239.3
3	4.63E+00	2	10	20	92.6
4	1.21E+01	1.5	13	19.5	236.1
1,000 PFU Dose Group 2					
5	2.98E+02	1.9	8	15.2	4528.3
6	3.44E+02	2.2	7	15.4	5296.3
7	2.93E+01	1.5	10	15	440
8	2.55E+02	2.2	7	15.2	3873.4
9	1.89E+02	2.8	5	14.1	2670.6
10	1.80E+02	2	7	14.1	2530.1
11	NA	1.3	15	19.5	0
12	8.53E+01	0.74	26	19.2	1633.7
13	1.02E+02	0.8	24	19.2	1957.6
14	9.52E+01	0.93	21	19.5	1856
10,000 PFU Dose Group 3					
15	2.21E+02	0.8	26	20.8	4598.3
16	7.04E+02	2.08	10	20.8	14644.1
17	1.57E+02	1.41	15	21.2	3316.1
18	3.01E+02	0.87	24	20.9	6276.1

Table 2: Aerosol particle size reported in aerodynamic diameter with individual geometric standard deviations (Top). Aerodynamic diameter distribution. Sample was taken during a large particle EBOV aerosol exposure. MMAD: 13.2 μm , GSD: 1.28. (Bottom).

Particle Size Distribution Averages		
Dose Group (PFU)	Aerodynamic Diameter (μm)	Geometric Standard Deviation
Group 1, 100	13.9	1.30
Group 2, 1,000	12.8	1.29
Group 3, 10,000	12.6	1.37
Average	13.1	1.32
STDEV	0.70	0.04



Clinical Course of Rhesus Macaques Exposed to Ebola Virus Aerosol

Of the eighteen NHPs exposed to EBOV inhalation aerosol, six NHPs did not show any clinical signs or symptoms of disease or any immunological response to infection. These animals included all animals exposed to 100 PFU of EBOV and two animals in the 1000 PFU dose group (NHP 10 and NHP 13). Eight of ten animals receiving 1000 PFU and 4 of 4 receiving 10,000 PFU succumbed to EBOV disease with typical clinical signs or symptoms, clinical pathology changes, gross and histopathology lesions, and immunostaining results as observed with rhesus macaque IM model, but with a slight delay in time to death versus IM challenge with the same virus. In this study, 11 of 12 (92%) animals succumbing to EBOV infection survived to or beyond PID 9, including single animals surviving to PID 10 or 11 (**Figure 1**).

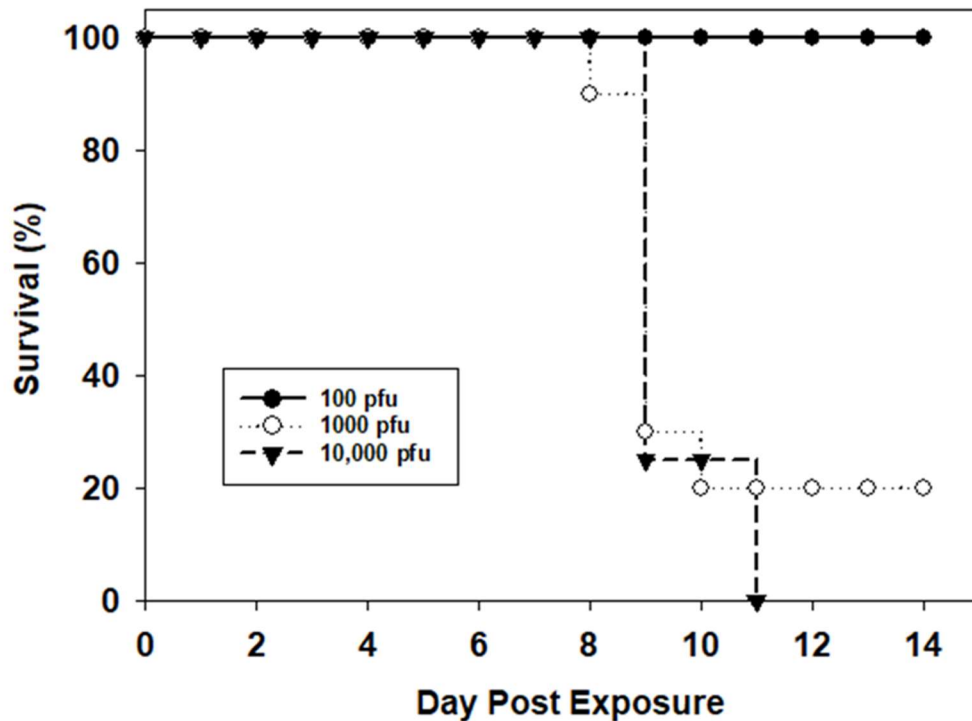


Figure 1: Mean time to death for large particle EBOV aerosol challenge in NHPs. Each line represents a dose group.

Imaging

NHPs that succumbed to EVD showed an increase of FDG activity in the upper respiratory tract prior to succumbing to EVD. (**Figure 2**). Generally the spleen, kidneys, and liver also displayed an increase in FDG activity over time in EBOV infected NHPs. NHP lungs were unremarkable and FDG activity was minimal, demonstrating the deposition in the upper respiratory tract (**Figure 2, Figure 3**). An increase activity was also seen in NHPs that received a higher dose (**Figure 3**). Uninfected NHPs were unremarkable in regards to FDG activity throughout the study (**Figure 4**).

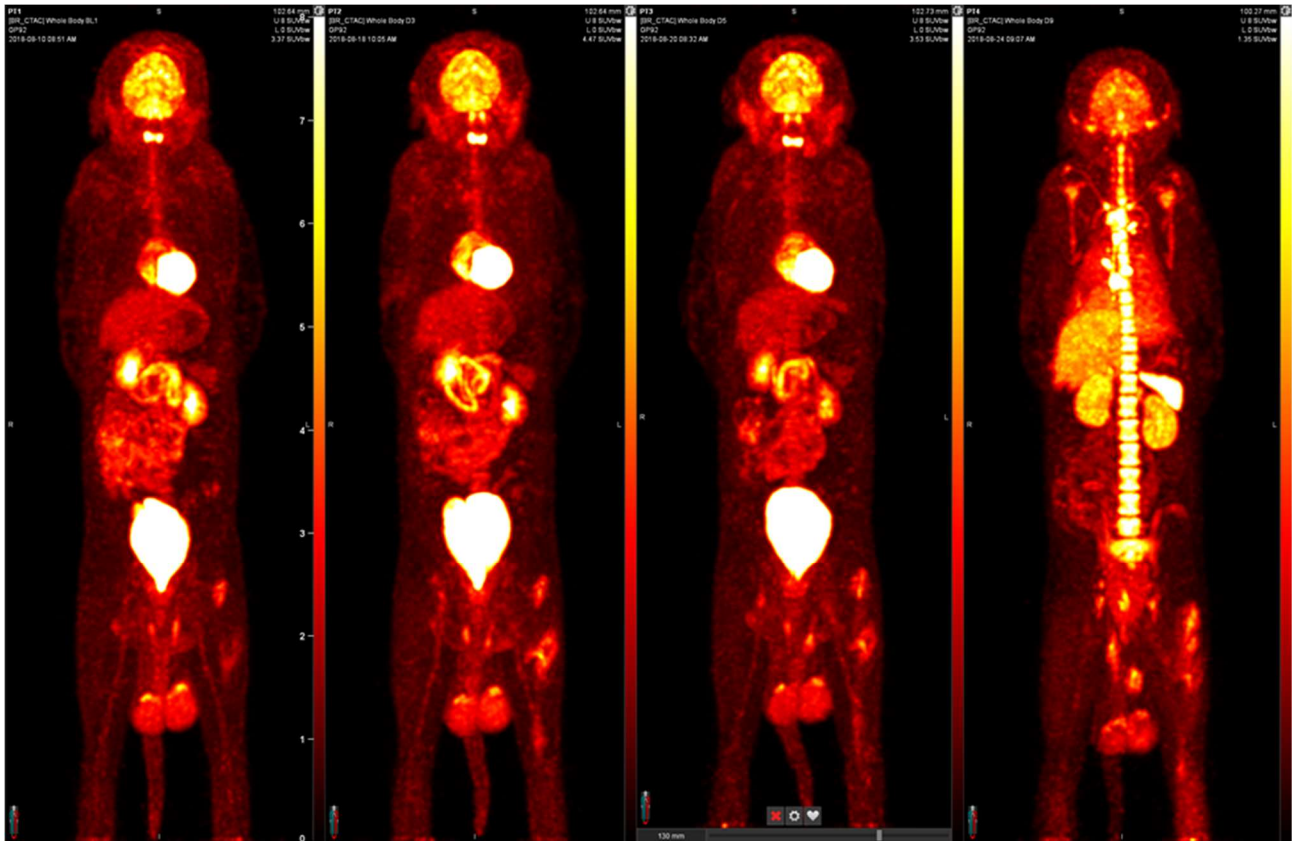


Figure 2: FDG PET images showing EVD progression over time. NHP 9 with a target dose of 1000 PFU. NHP's actual dose was 2670 PFU. Images above were taken at baseline and 3, 5, 7, and 9 PID. Imaging SUV 0-8.

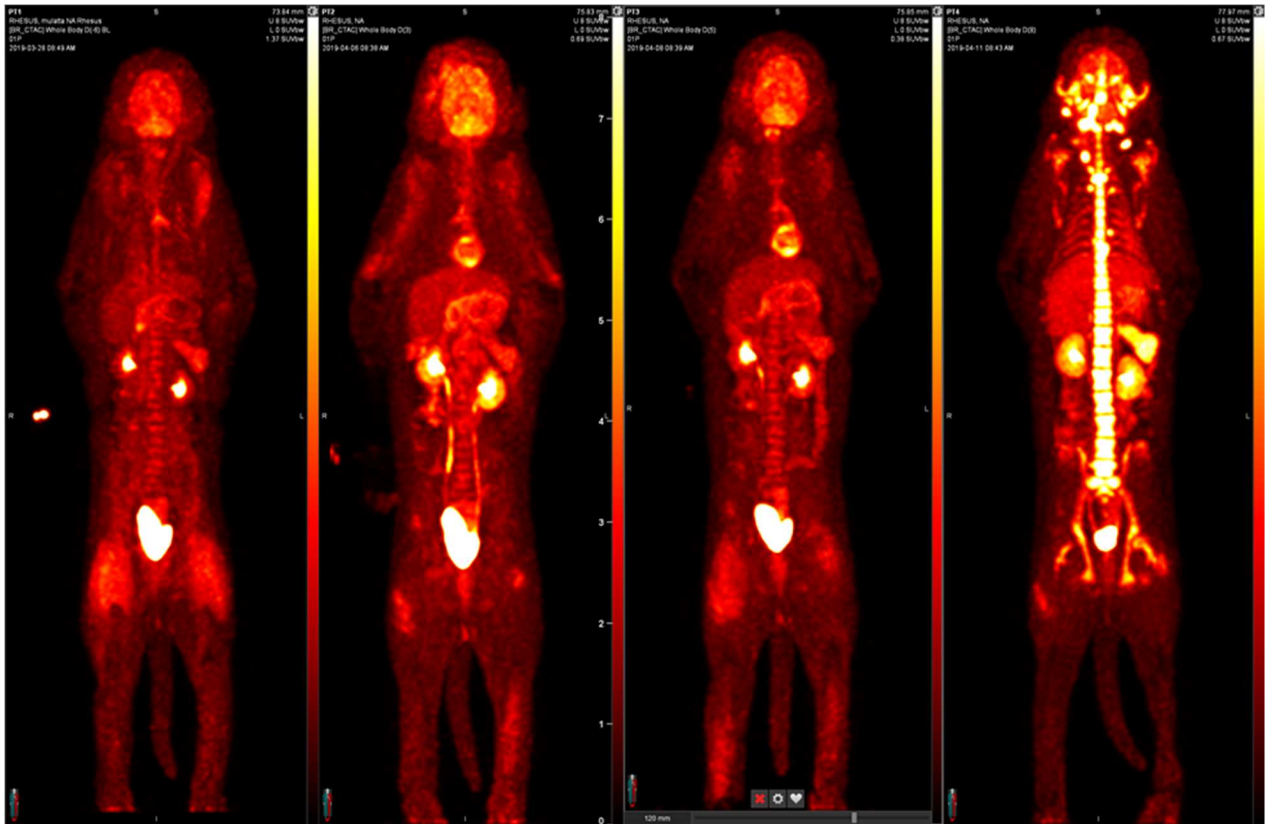


Figure 3: FDG PET images showing EVD progression over time. NHP 16 with a target dose 10,000 PFU. NHP's actual dose was 2670 PFU. Images above were taken at baseline and 3, 5, and 8 PID. Imaging SUV 0-8.

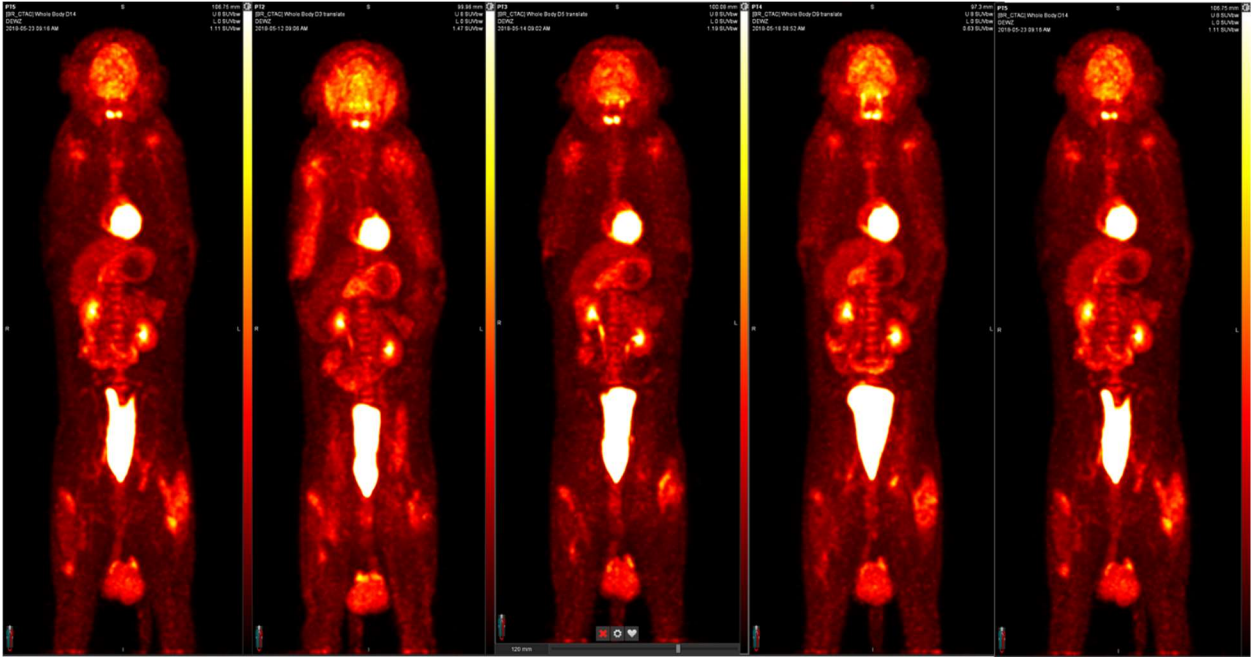


Figure 4: FDG PET images showing no clinical signs of EVD over time. NHP 1 with a target dose of 100 PFU. NHP's actual dose was 254 PFU. Day 14 Scan. SUV 0-8

Flow Cytometry

Generally, at PID 5, an increase in hematopoietic cells (CD45+) in the blood was most likely due to an increase in granulocytes (**Figure 5**). This observation is consistent with the complete blood count results. In the lymphoid compartment, B cells remained relatively consistent throughout infection (**Figure 6**), with a slight decrease seen in the 1000 PFU group (n = 7, excluding uninfected animals and one animal, NHP 10, with missing immunology samples from terminal phase).

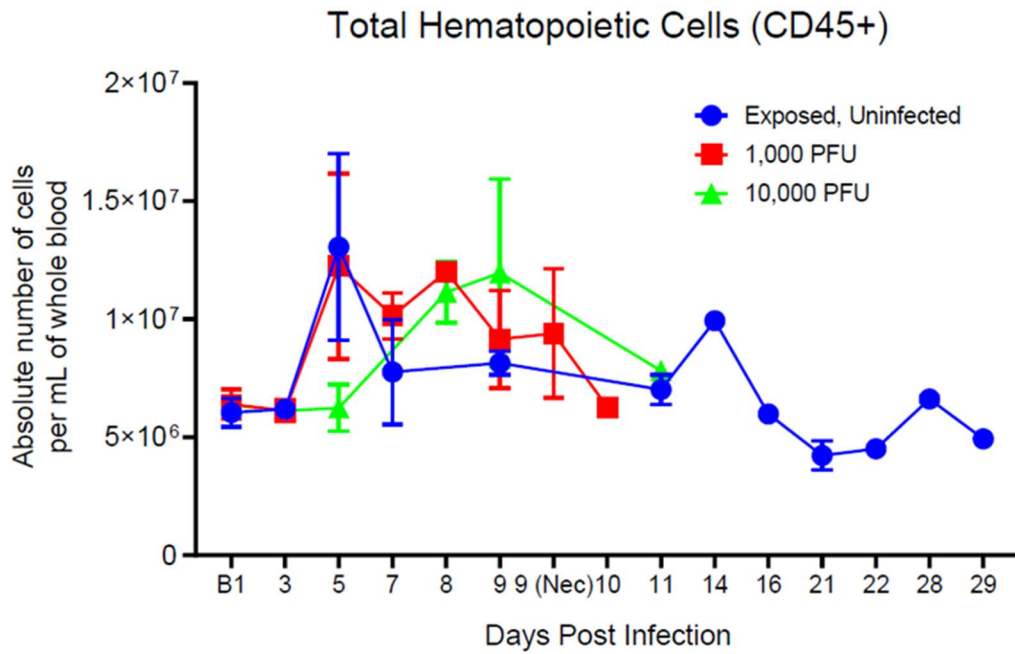


Figure 5: Absolute number of hematopoietic cells (CD45+) in whole blood over time for all dose groups.

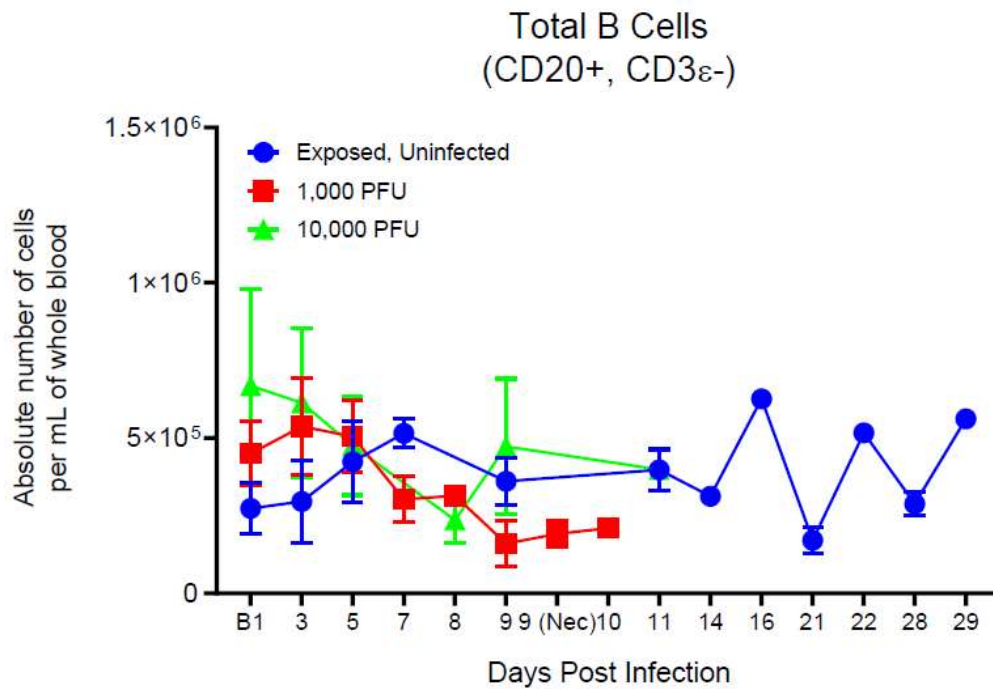


Figure 6: Absolute number of B cells (CD20+, CD3ε-) in whole blood over time for all dose groups.

In contrast, a decrease in T cells began at PID 3. This decrease was most pronounced for CD4 T cells, dropping to less than 5% of baseline at time of death (**Figure 7**). CD8 T cells remained rather stable during infection (**Figure 8**). The dramatic decrease of CD4 T cells led to an inverted CD4:CD8 T cell ratio, consistent with immune dysfunction. Interestingly, the 10,000 PFU group showed an inverted T cell ratio earlier than the 1,000 PFU group. Both T cell subsets displayed surface EBOV GP, particularly on CD4 T cells. This is likely due to toll like receptors binding to EBOV GP and not indicative of T cells becoming infected.

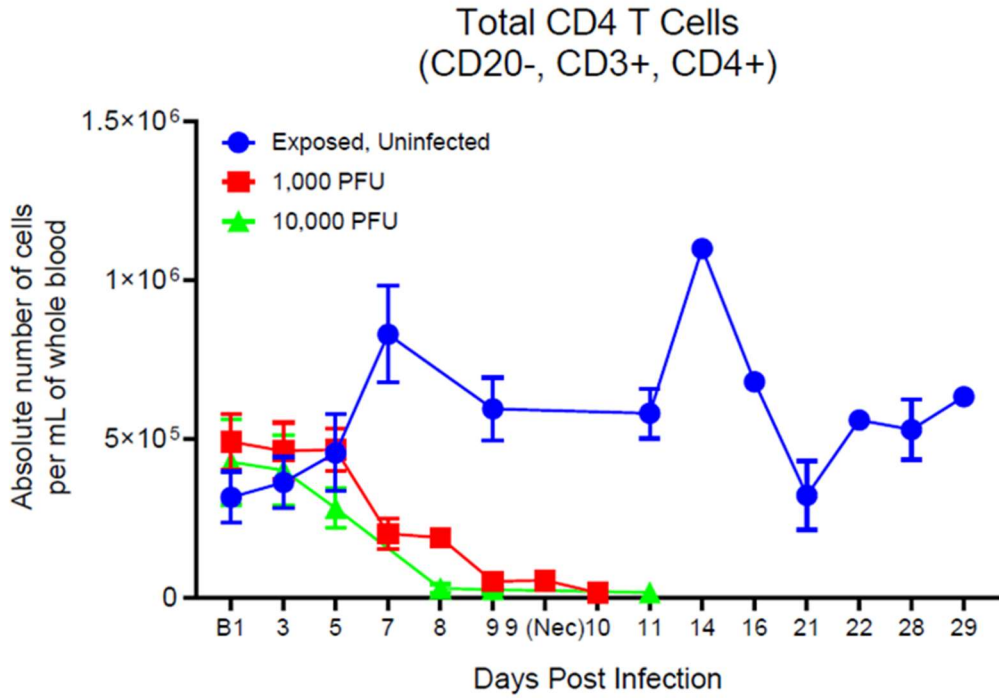


Figure 7: Absolute number of CD4 T cells (CD20-, CD3+, CD4+) in whole blood over time for all dose groups.

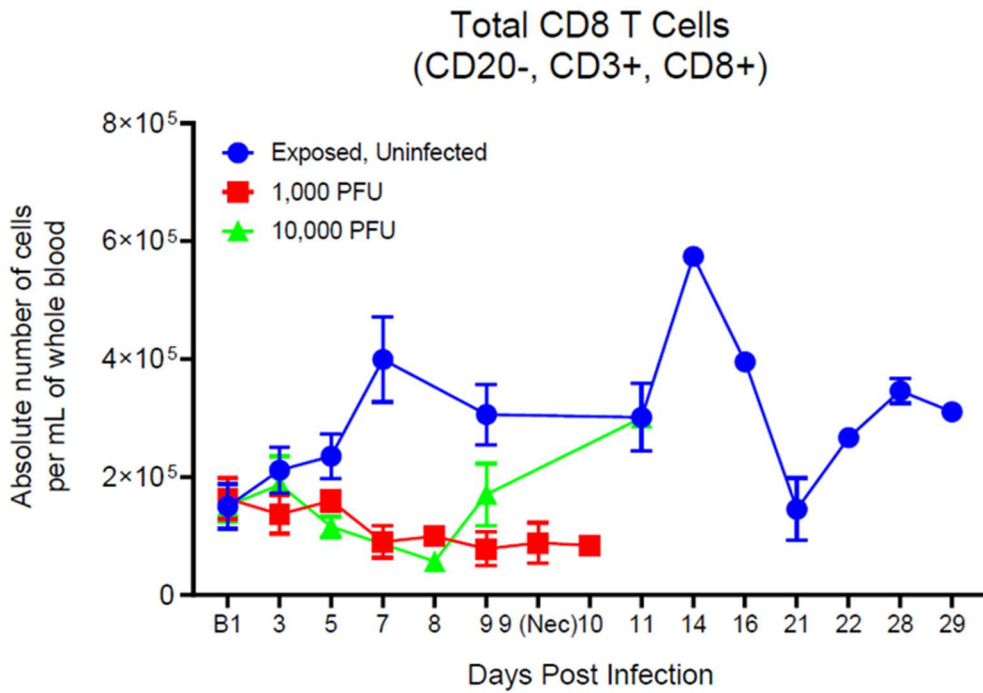


Figure 8: Absolute number of CD8 T cells (CD20-, CD3+, CD8+) in whole blood over time for all dose groups.

Natural killer (NK) cells decreased slightly during infection (**Figure 9**). However, the decrease in circulating NK cells is unlikely to be due to apoptosis, as these cells showed little annexin V staining and faint staining for EBOV-GP.

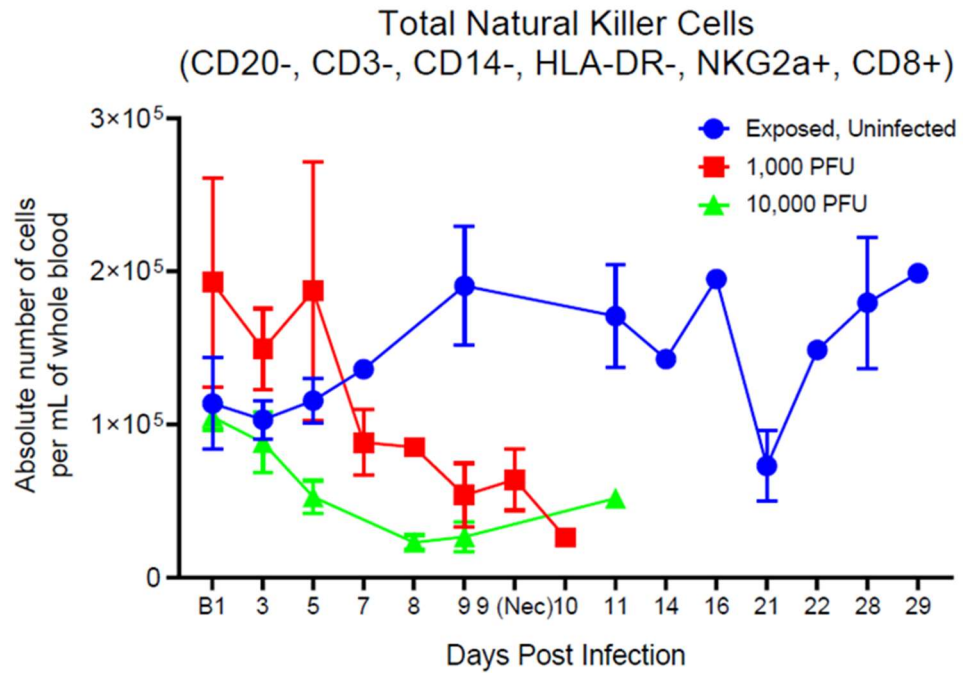


Figure 9: Absolute number of NK cells (CD20-, CD3-, CD14-, HLA-DR-, NKG2a+, CD8+) in whole blood over time for all dose groups.

In the myeloid compartment, a slight increase in both monocytes and CD163+ macrophages was noted in the 1000 PFU group. Monocytes did not show much EBOV-GP or Annexin V staining during infection collected from either the 1,000 PFU group or the 10,000 PFU group. Whereas CD163+ macrophages made up a very small number of CD45+ cells in the blood, an increase was observed from PID 5 to 7 and PID 9 to 10 in

the 1,000 PFU group. Macrophages also showed annexin V staining at necropsy. Compared to monocytes, EBOV GP was present in macrophages earlier during infection. Lastly, myeloid dendritic cells decreased slightly in the 10,000 PFU group, and little annexin V staining of these cells was observed at necropsy in most animals. However, an increase in EBOV-GP staining of myeloid dendritic cells was observed in some animals at necropsy.

Lung tissue and BAL fluid were collected at necropsy from each NHP, and cell phenotypes were determined using methods similar to that used in the whole blood. One major difference was the differentiation between lung macrophage subtypes (interstitial vs. alveolar macrophages). B cells made up the majority of lymphocytes isolated from the lung tissue and the BAL fluid. In the lung, CD4 T cells had the most EBOV-GP staining, and CD8 T cells were stained to a lesser extent, similar to whole blood. Both B cells and CD4 T cells had appreciable annexin V staining in the lung. Myeloid compartment was dominated by monocytes and granulocytes at necropsy. Whereas interstitial and alveolar macrophages made up a small percentage of the myeloid cells in the lung, the majority of EBOV-GP staining was from alveolar macrophages.

The BAL fluid was primarily made up of alveolar macrophages, although lymphocytes and granulocytes were also detected. EBOV-GP staining was equivalent between CD4 and CD8 T cells in the BAL fluid. Like the lungs, the alveolar macrophages showed similar percentages of EBOV-GP staining. Differences in cell phenotypes post exposure were unable to be determined without uninfected control tissue.

Cytokine Analysis

During EBOV infection in these cohorts of NHPs, inflammatory mediators (e.g., interleukin [IL]-1 β , IL-6, IL-8, IL-18, tumor necrosis factor-alpha [TNF- α]) were elevated. TNF- α and inflammatory ILs started to increase at PID 3 and 5, respectively. Additionally, inflammatory chemoattractant chemokines were increased during EBOV infection (IL-8, monocyte chemoattractant protein-1 [MCP-1], macrophage inflammatory protein-1 alpha [MIP-1 α], and MIP-1 β). GM-CSF and G-CSF are cytokines involved in stimulating the innate immune cells such as granulocytes and macrophages corresponding to the neutrophilia seen in NHP EVD models.

Overall, the cytokine data are indicative of immune dysregulation that leads to life-threatening organ dysfunction “cytokine storm.” Th1 cytokines IFN γ , IL-2, and TNF- α were all elevated during EVD, and Th2 cytokine IL-13 was elevated during late infection. Other Th2 cytokines, IL-4 and IL-5, were not affected. An increase in anti-inflammatory cytokines IL-10 and IL-1Ra was also seen following aerosol EBOV challenge after PID 5.

Hematology and Clinical Chemistry

Total white blood cell counts generally increased around PID 7–9, mostly due to increased neutrophils. In approximately half of animals, these counts continued to increase to termination, whereas in the remaining animals, a terminal decline of white blood cell counts was noted. Lymphocytes generally declined to PID 7–9, with a slight increase at termination. Monocytes generally increased to PID 7–8, with a monocytosis in four animals, followed by marked declines (**Figure 10**).

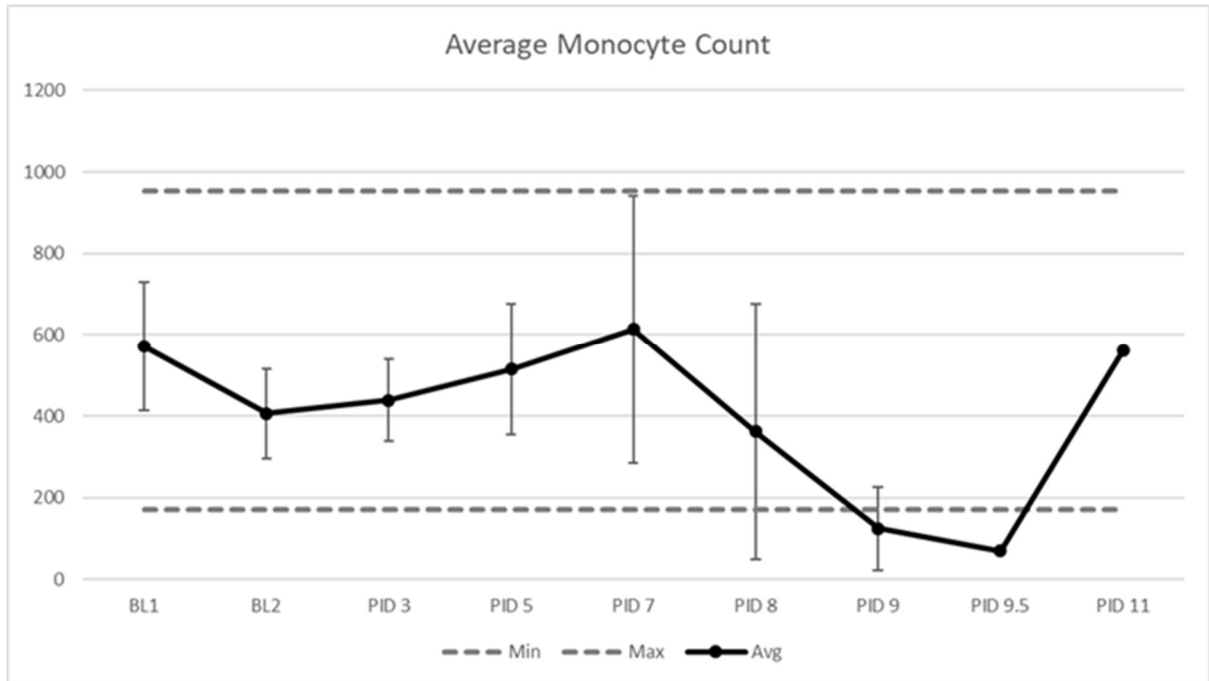


Figure 10: Average monocyte counts over time for EBOV infected NHPs.

Platelet counts declined for all animals during the course of disease. All animals were below normal reference interval at termination, with 7/12 animals below 100,000/uL (the generally accepted threshold for thrombocytopenia) (**Figure 11**). Both the hematocrit and reticulocyte counts generally decreased during the course of disease, consistent with blood loss and inability of the bone marrow to effectively regenerate. In a few animals, hemoconcentration was noted at termination, consistent with dehydration.

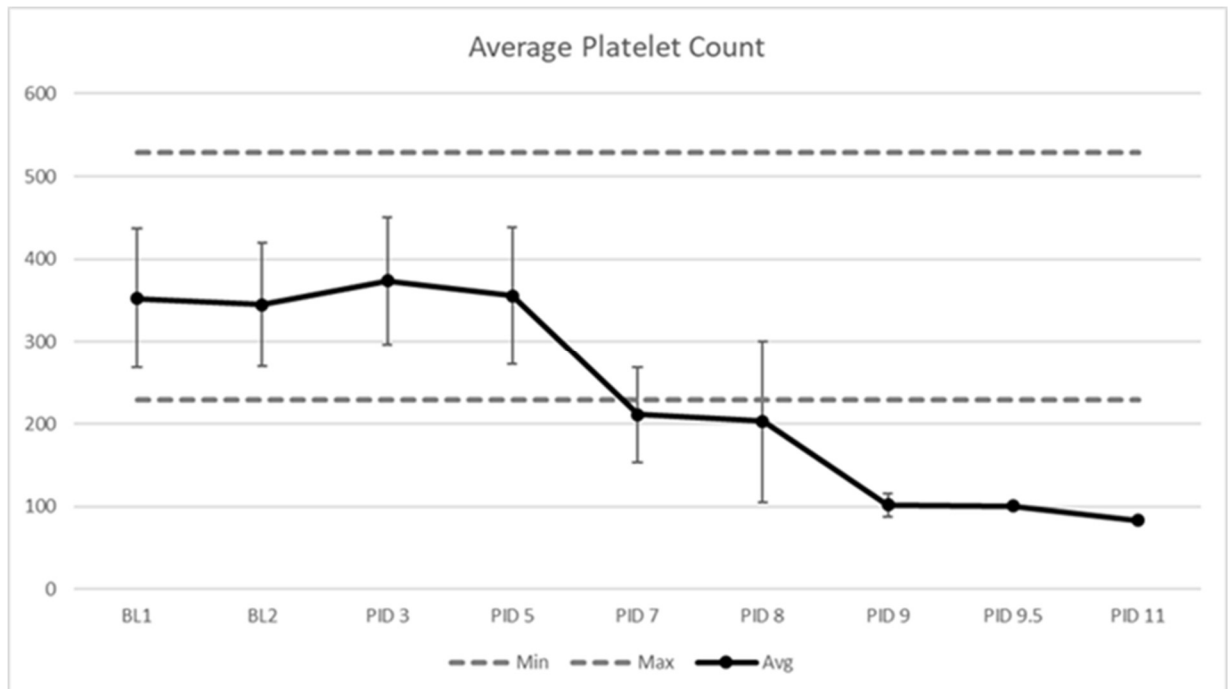


Figure 11: Average platelet counts over time for EBOV Infected NHPs.

ALT and AST increased substantially beginning at PID 5–9. Albumin declined during the course of disease, likely a combination of diminished synthesis as well as increased vascular permeability (**Figure 12, 13**). Hypoalbuminemia was noted in 17/18 animals by PID 8–9, and all animals were hypocalcemic (even after correcting for hypoproteinemia) by PID 9. Total bilirubin increased in all animals at termination, and one animal (NHP 15) was grossly icteric. All animals were azotemic by PID 9.

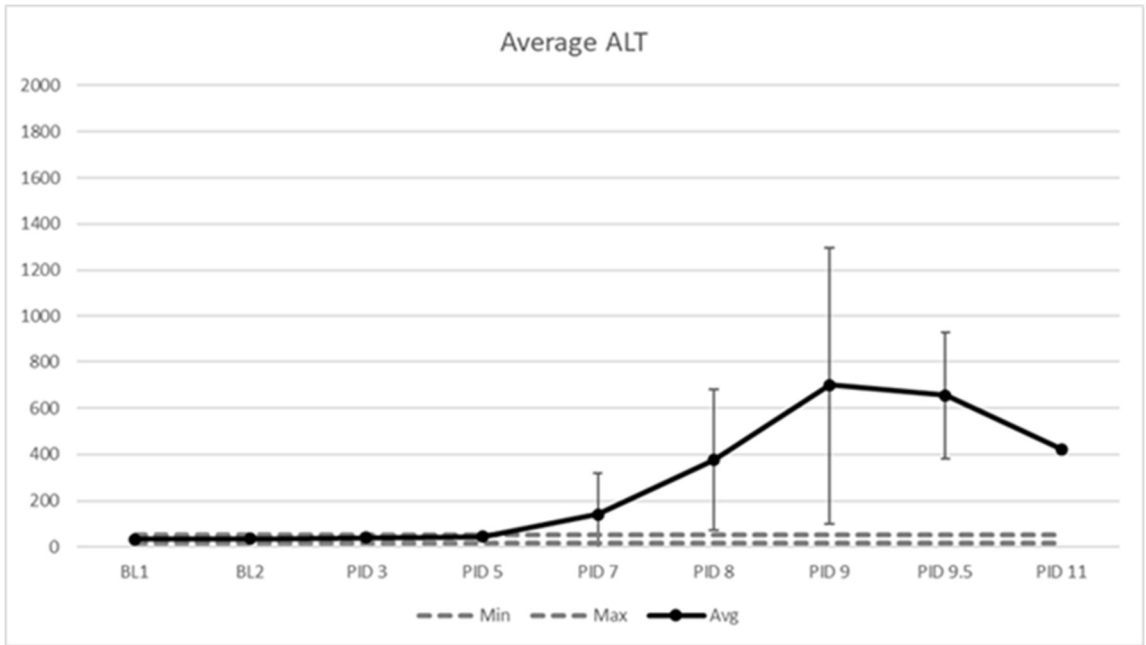


Figure 12: Average ALT over time for EBOV Infected NHPs.

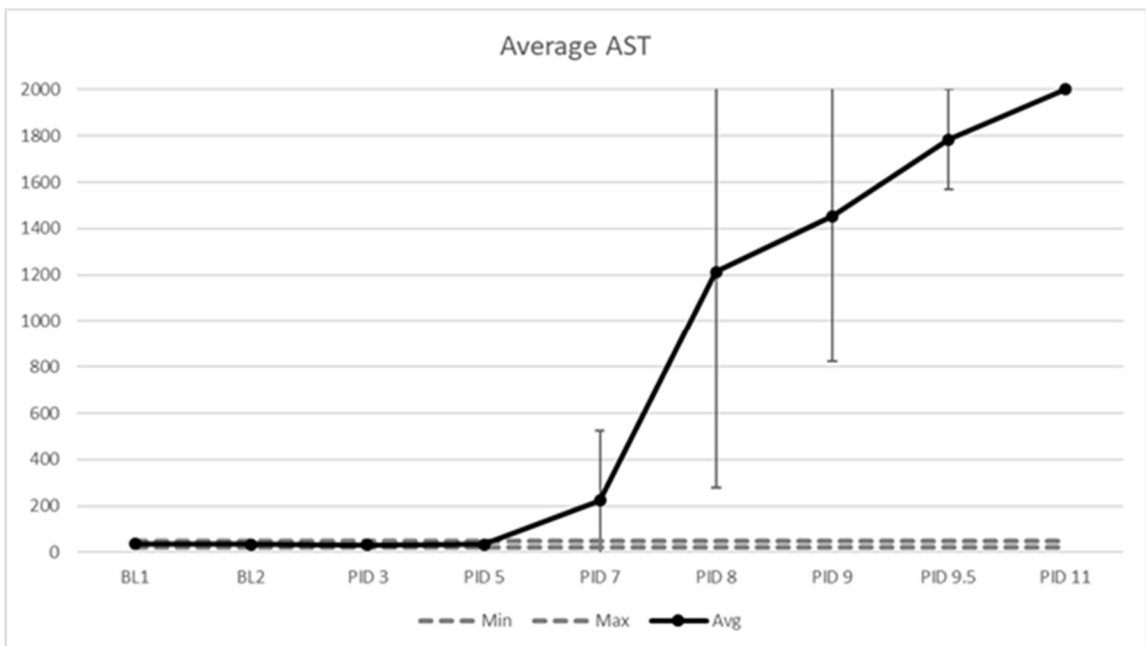


Figure 13: Average AST over time for EBOV Infected NHPs.

Anatomic Pathology

Gross and histologic lesions in the 12 animals that succumbed to acute infection were generally consistent with what was observed with 1000 PFU EBOV/Makona-C05 given IM in the rhesus macaque model at this institute, except that cervical and tracheobronchial rather than axillary lymph nodes were most severely affected following aerosol exposure (**Figure 14, Figure 15**). As typically observed previously, hepatosplenomegaly with necrosis, widespread thrombosis, and cutaneous petechiae were noted. In most animals, the necrosis score in cervical lymph nodes exceeded or was on par with tracheobronchial nodes. This pattern was conspicuously reversed in one animal that may have been exposed to small particles generated during aerosol exposure (NHP 11). However, a similar reversal was also present in two other animals (NHP 16 and NHP 18).

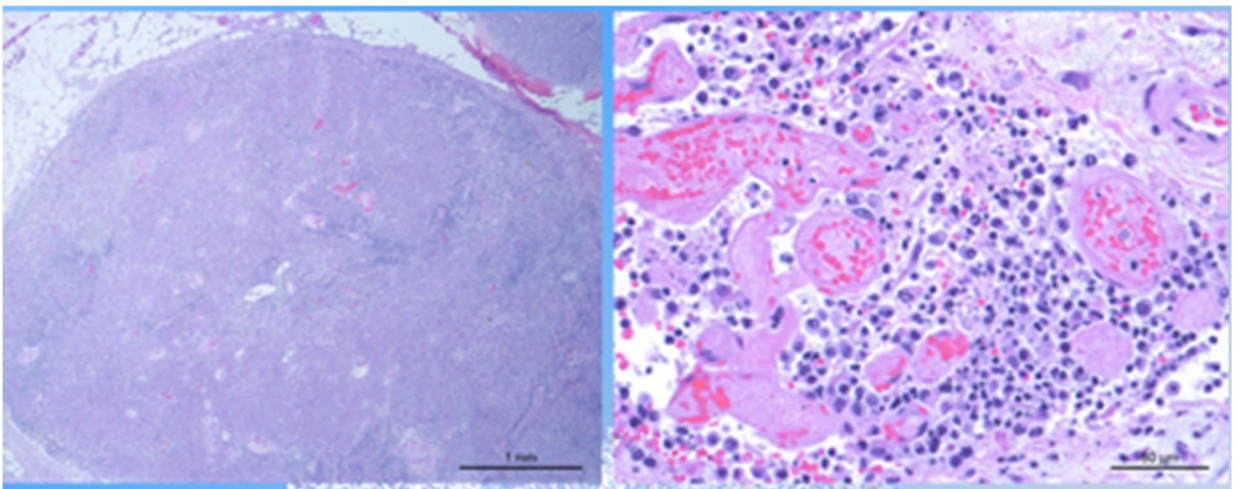


Figure 14: IHC staining of the tracheal/bronchial lymph nodes of Ebov infected NHPs. Localized UTR infection is indicated from large particle EBOV exposure.

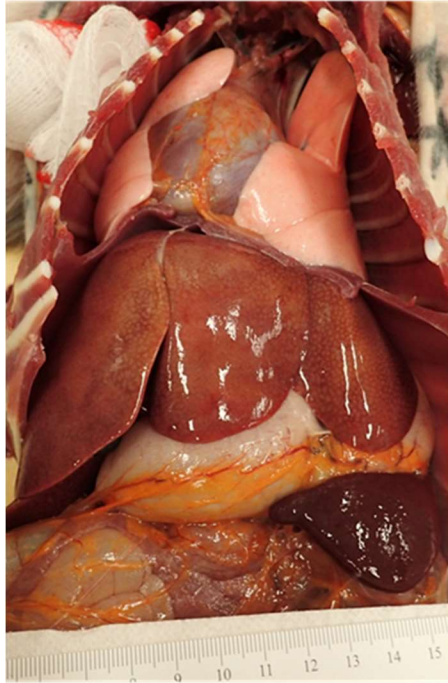


Figure 15: Pathology from large particle EBOV exposure is consistent with NHPs receiving an IM EBOV exposure. The spleen and liver is markedly enlarged with rounded edges. The red pulp is expanded by abundant necrosis and fibrin.

In all but three animals, a mild multifocal acute rhinitis/sinusitis was noted, consisting of edema and neutrophilic inflammatory exudates with scant acute hemorrhage. Tracheal mucosal lesions included lymphoid depletion of the mucosa-associated lymphoid tissue, edema, and histiocytic infiltrates with necrosis/apoptosis. Lungs were grossly unremarkable. Histologically, lungs in all 11/12 animals were consistent with what is observed with intra-muscular exposure (**Figure 4, 16**). In a single animal (NHP 14), a moderate acute inflammatory process centered on the terminal bronchioles and adjacent alveoli was noted, with a polymicrobial bacterial population and large rafts of cornified squamous cells (consistent with aspiration pneumonia).

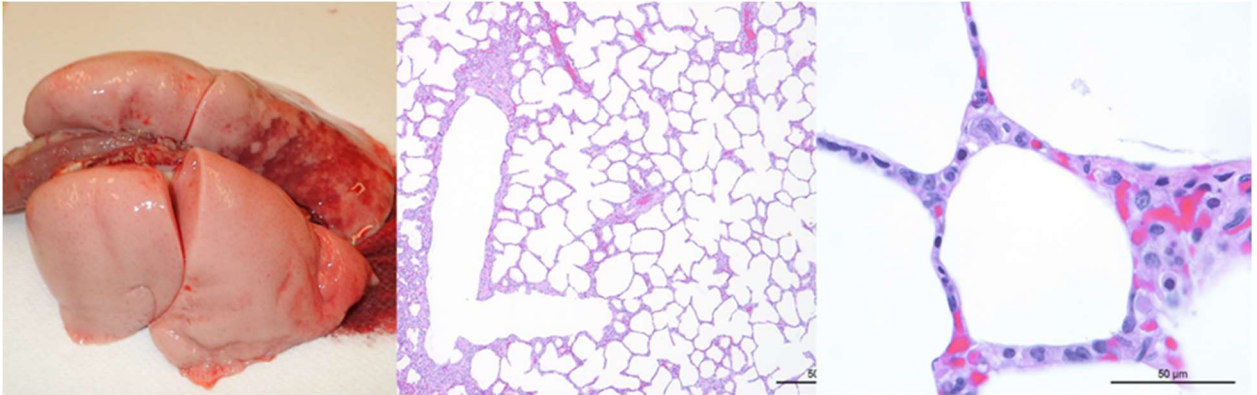


Figure 16: Gross pathology (left) and IHC staining (right) for the lungs from large particle EBOV exposure is consistent with what is observed with an IM EBOV exposure. Lungs were diffusely pink and spongy throughout, which is consistent with a large particle aerosol exposure.

Lesions in the eyes, including thrombosis of the ciliary pars plicata, were generally consistent with what has been seen in IM EBOV exposure studies, although uveitis (cyclitis) in one animal (NHP 16) was significantly different/worse than what has been observed in other studies (**Figure 17**). In two animals (NHP 7 and NHP 9), widespread necrosis and hemorrhage of the adrenal cortex (adrenal apoplexy) were observed. No significant lesions were found in the brain, including olfactory bulbs/nerves.

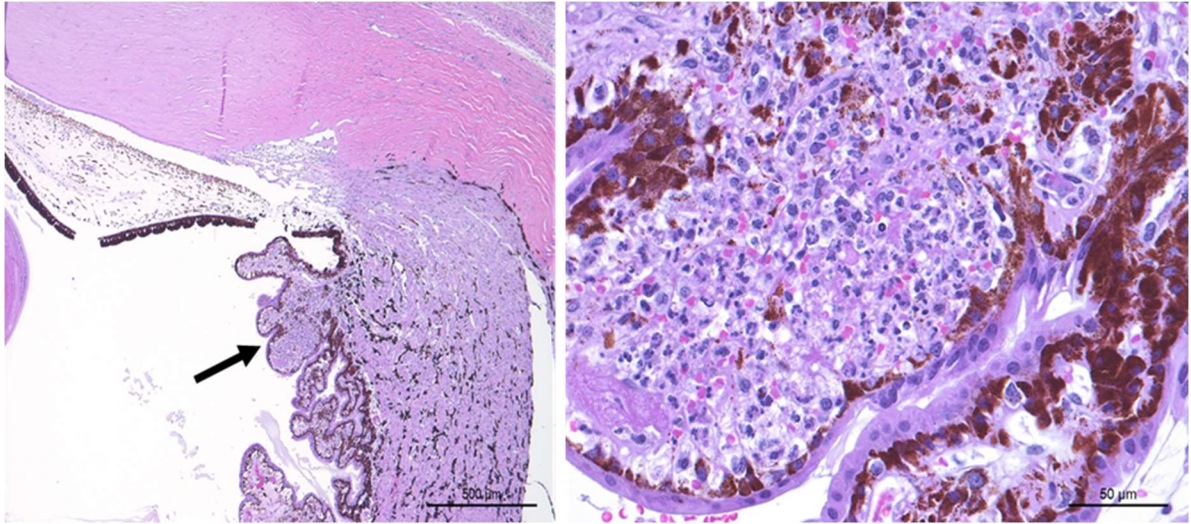


Figure 17: IHC staining of the eye of NHP 16 showing bilateral anterior uveitis (Day 9, 14,644 PFU).

Immunohistochemistry and RNAscope in situ hybridization, including distribution and cell types affected, were generally consistent throughout the study in regards to NHPs infected by large particle EBOV. Positive immunolabeling of epithelia was generally more prevalent in the nasal cavity and cranial (proximal) trachea than distal trachea or mainstem bronchi.

DISCUSSION

Controlling the site of particle deposition of aerosolized pathogens may play a key role in altering disease course, presentation, and time to death. Small particles that deposit within the alveolar regions of the lung bypass the innate physical defense barriers of the upper respiratory system such as mucociliary clearance (Dabisch 2017). Previous studies have shown a correlation between particle size, particle deposition, and lethality of various pathogens (Druett 1953, Day and Berendt 1972, Johnson 2016). Mucociliary clearance is a mechanism used by ciliated airway epithelium cells and secretory cells in the upper airways as a host defense against pathogens in the lungs. (Vareille 2011). Airway epithelial cells also regulate both the innate and adaptive immunity through the production of functional molecules and interactions with cells of the immune system (Hiemstra 2001).

Overall, the disease course of animals receiving aerosolized EBOV are consistent with lethal EVD in rhesus macaques, and similar to results seen following IM challenge. Twelve animals were successfully infected and succumbed to EBOV disease had typical clinical signs and clinical pathology changes as the IM rhesus macaque model, but had a slight delay in time to death compared to the IM model. At this institution 72 untreated Indian origin rhesus macaques that received the 1000 pfu IM dose of EBOV/Makona-C05 and the average time to death was 7.73 days ($SD \pm 0.92$). Only 7 of 72 (9.7%) survived to at least PID 9, three of which survived to PID 10 (4.2%). No untreated animal has previously survived to day 11 and succumbed to EVD.

Lesions and immunostaining in the upper (nasal cavity, oropharynx and cranial trachea) versus lower respiratory tract (caudal trachea, mainstem bronchi and lungs) were generally consistent with a large particle route of exposure. Lesions in the lungs were generally similar to what is seen in the IM challenge model. In small particle aerosol studies (Twenhafel 2013), unpublished data, inflammation and hemorrhage of the pulmonary bronchioles and/or interstitium were noted in some animals, a feature absent from this study.

Whereas liver lesions were generally consistent with those seen in the IM model, two notable distinctions were observed. First, increased mixed leukocytic inflammation was associated with liver necrosis in many of these aerosolized EBOV-infected animals relative to what is generally observed following IM challenge. Second, in four animals, hepatocellular necrosis affected <5% of the liver parenchyma, versus the 10–25% that is typical for IM challenge with EBOV. These discrepancies may or may not be related to the alternative route of exposure and/or increased time to death.

Overall, changes in immune cell populations are consistent with lethal EVD, and similar to results seen following IM challenge. Decreases in the T-lymphocytes, myeloid cells, and NK cells were observed. T-cell depletion may be consistent with EBOV GP cell surface staining on both T cell subsets that directly trigger T-lymphocyte apoptosis, as indicated by increased annexin V staining, and death through toll-like receptors-4 binding and upregulation of caspase 9 (Iampietro 2017, Younan). Despite the decrease in CD4⁺ T cell numbers during late infection, some associated Th1 and Th2 cytokines increased during EBOV infection. Th1 cytokines, IFN γ , IL-2, and TNF α , were all elevated during EBOV infection, and Th2 cytokine, IL-13 increased during late infection.

Th1 cytokines are likely to be produced by other cells, such as CD8 T cells (IL-2 and IFN γ), NK cells (IFN γ and TNF α), and macrophages (TNF α). IFN γ has been shown in the literature to be important for combating EBOV. Due to lymphopenia and decreasing CD4 T cell numbers during EVD, other cell populations such as NK cells, basophils, eosinophils, and mast cells could be the source of this increase in IL-13.

During EBOV infection in these cohorts of monkeys, inflammatory mediators, such as (IL)-1 β , IL-6, IL-8, IL-18, and TNF- α were elevated during infection. The IL-1 β and IL-18 axis are induced in the innate response through activation of the NLRP3 inflammasome cleaving caspase-1, which in turn cleaves pro-IL-1 β and pro-IL-18. GM-CSF and G-CSF are cytokines involved in stimulating the innate immune cells such as granulocytes and macrophages corresponding to the neutrophilia seen during EBOV infection.

This study has several limitations. Whereas the EBOV-GP staining results from CD4 and CD8 T cell are interesting, caution should be applied when interpreting these results. Flow cytometry cannot distinguish between the presence of live virus or viral antigens. Additionally, distinguishing between positive versus negative staining of highly auto-fluorescent cells (i.e., macrophages and granulocytes) is difficult. Annexin V staining alone cannot distinguish between apoptotic and necrotic cells. Uninfected control tissues would be necessary to determine changes in tissue phenotypes. Lastly, baseline CD4:CD8 T cell ratios should be determined for rhesus macaques, as sources in the literature are scarce. Baseline values for all circulating cell phenotypes would be helpful for future studies.

Future research is needed to further investigate the correlation between aerosol particle size and the infectious dose of large particle EBOV in NHPs. This large particle model may be useful in testing therapeutics that require a delayed time (in comparison to an IM model) to infection to mimic that of human EVD.

REFERENCES

- Alves DA, Glynn AR, Steele KE, Lackemeyer MG, Garza NL, Buck JG, et al. Aerosol exposure to the Angola strain of Marburg virus causes lethal viral hemorrhagic fever in cynomolgus macaques. *Vet Pathol.* 2010;47(5):831-51.
- Barnewall RE, Fisher DA, Robertson AB, Vales PA, Knostman KA, Bigger JE. Inhalational monkeypox virus infection in cynomolgus macaques. *Front Cell Infect Microbiol.* 2012;2:117.
- Bausch DG, Towner JS, Dowell SF, Kaducu F, Lukwiya M, Sanchez A, et al. Assessment of the risk of Ebola virus transmission from bodily fluids and fomites. *J Infect Dis.* 2007;196 Suppl 2:S142-7.
- Besch TK, Ruble DL, Gibbs PH, Pitt ML. Steady-state minute volume determination by body-only plethysmography in juvenile rhesus monkeys. *Lab Anim Sci.* 1996;46(5):539-44.
- Cheng YS, Irshad H, Kuehl P, Holmes TD, Sherwood R, Hobbs CH. Lung deposition of droplet aerosols in monkeys. *Inhal Toxicol.* 2008;20(11):1029-36.
- Cooper TK, Sword J, Johnson JC, Bonilla A, Hart R, Liu DX, et al. New insights into Marburg virus disease pathogenesis in the rhesus macaque model. *J Infect Dis.* 2018;218(suppl_5):S423-S33.
- Dabisch PA, Xu Z, Boydston JA, Solomon J, Bohannon JK, Yeager JJ, et al. Quantification of regional aerosol deposition patterns as a function of aerodynamic particle size in rhesus macaques using PET/CT imaging. *Inhal Toxicol.* 2017;29(11):506-15.
- Day WC, Berendt RF. Experimental tularemia in *Macaca mulatta*: relationship of aerosol particle size to the infectivity of airborne *Pasteurella tularensis*. *Infect Immun.* 1972;5(1):77-82.
- Druett HA, Henderson DW, Packman L, Peacock S. Studies on respiratory infection. I. The influence of particle size on respiratory infection with anthrax spores. *J Hyg (Lond).* 1953;51(3):359-71.
- Formenty P, Leroy EM, Epelboin A, Libama F, Lenzi M, Sudeck H, et al. Detection of Ebola virus in oral fluid specimens during outbreaks of Ebola virus hemorrhagic fever in the Republic of Congo. *Clin Infect Dis.* 2006;42(11):1521-6.
- Gralton J, Tovey E, McLaws ML, Rawlinson WD. The role of particle size in aerosolised pathogen transmission: a review. *J Infect.* 2011;62(1):1-13.

- Hartman AL, Powell DS, Bethel LM, Caroline AL, Schmid RJ, Oury T, et al. Aerosolized Rift valley fever virus causes fatal encephalitis in African green monkeys and common marmosets. *J Virol*. 2014;88(4):2235-45.
- Hiemstra PS. Epithelial antimicrobial peptides and proteins: their role in host defence and inflammation. *Paediatr Respir Rev*. 2001;2(4):306-10.
- Hinds W. *Aerosol technology: properties, behavior, and measurement of airborne particles*. 2 ed. Hoboken, NJ: John Wiley & Sons; 1999.
- Iampietro M, Younan P, Nishida A, Dutta M, Lubaki NM, Santos RI, et al. Ebola virus glycoprotein directly triggers T lymphocyte death despite of the lack of infection. *PLoS Pathog*. 2017;13(5):e1006397.
- Jaax N, Jahrling P, Geisbert T, Geisbert J, Steele K, McKee K, et al. Transmission of Ebola virus (Zaire strain) to uninfected control monkeys in a biocontainment laboratory. *Lancet*. 1995;346(8991-8992):1669-71.
- Johnson RF, Hammoud DA, Perry DL, Solomon J, Moore IN, Lackemeyer MG, et al. Exposure of rhesus monkeys to cowpox virus Brighton Red by large-particle aerosol droplets results in an upper respiratory tract disease. *J Gen Virol*. 2016;97(8):1942-54.
- Lee KM, Chiu KB, Sansing HA, Didier PJ, Ficht TA, Arenas-Gamboa AM, et al. Aerosol-induced brucellosis increases TLR-2 expression and increased complexity in the microanatomy of astroglia in rhesus macaques. *Front Cell Infect Microbiol*. 2013;3:86.
- Nalca A, Livingston VA, Garza NL, Zumbrun EE, Frick OM, Chapman JL, et al. Experimental infection of cynomolgus macaques (*Macaca fascicularis*) with aerosolized monkeypox virus. *PLoS One*. 2010;5(9).
- Osterholm MT, Moore KA, Kelley NS, Brosseau LM, Wong G, Murphy FA, et al. Transmission of Ebola viruses: what we know and what we do not know. *MBio*. 2015;6(2):e00137.
- Perry DL, Huzella LM, Bernbaum JG, Holbrook MR, Jahrling PB, Hagen KR, et al. Ebola Virus localization in the macaque reproductive tract during acute Ebola virus disease. *Am J Pathol*. 2018;188(3):550-8.
- Piercy TJ, Smither SJ, Steward JA, Eastaugh L, Lever MS. The survival of filoviruses in liquids, on solid substrates and in a dynamic aerosol. *J Appl Microbiol*. 2010;109(5):1531-9.
- Raabe OG, Al-Bayati MA, Teague SV, Rasolt A. Regional deposition of inhaled monodisperse coarse and fine aerosol particles in small laboratory animals. *Ann Work Expo Health*. 1988;32(inhaled_particles_VI):53-63.

Reed DS, Lackemeyer MG, Garza NL, Sullivan LJ, Nichols DK. Aerosol exposure to Zaire ebolavirus in three nonhuman primate species: differences in disease course and clinical pathology. *Microbes Infect.* 2011;13(11):930-6.

Richards GA, Murphy S, Jobson R, Mer M, Zinman C, Taylor R, et al. Unexpected Ebola virus in a tertiary setting: clinical and epidemiologic aspects. *Crit Care Med.* 2000;28(1):240-4.

Rodriguez LL, De Roo A, Guimard Y, Trappier SG, Sanchez A, Bressler D, et al. Persistence and genetic stability of Ebola virus during the outbreak in Kikwit, Democratic Republic of the Congo, 1995. *J Infect Dis.* 1999;179 Suppl 1:S170-6.

Rowe AK, Bertolli J, Khan AS, Mukunu R, Muyembe-Tamfum JJ, Bressler D, et al. Clinical, virologic, and immunologic follow-up of convalescent Ebola hemorrhagic fever patients and their household contacts, Kikwit, Democratic Republic of the Congo. Commission de Lutte contre les Epidemies a Kikwit. *J Infect Dis.* 1999;179 Suppl 1:S28-35.

Twenhafel NA, Mattix ME, Johnson JC, Robinson CG, Pratt WD, Cashman KA, et al. Pathology of experimental aerosol Zaire ebolavirus infection in rhesus macaques. *Vet Pathol.* 2013;50(3):514-29.

Vareille M, Kieninger E, Edwards MR, Regamey N. The airway epithelium: soldier in the fight against respiratory viruses. *Clin Microbiol Rev.* 2011;24(1):210-29.

Wang L, Shi W, Joyce MG, Modjarrad K, Zhang Y, Leung K, et al. Evaluation of candidate vaccine approaches for MERS-CoV. *Nat Commun.* 2015;6:7712.

Yeager JJ, Facemire P, Dabisch PA, Robinson CG, Nyakiti D, Beck K, et al. Natural history of inhalation melioidosis in rhesus macaques (*Macaca mulatta*) and African green monkeys (*Chlorocebus aethiops*). *Infect Immun.* 2012;80(9):3332-40.

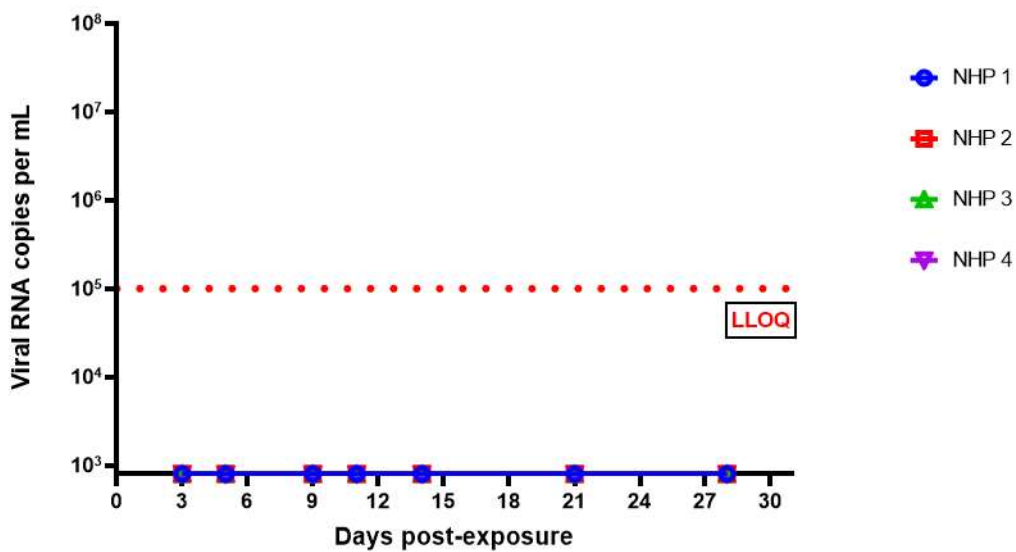
Younan P, Santos RI, Ramanathan P, Iampietro M, Nishida A, Dutta M, et al. Ebola virus-mediated T-lymphocyte depletion is the result of an abortive infection. *PLoS Pathog.* 2019;15(10):e1008068.

Zumbrun EE, Bloomfield HA, Dye JM, Hunter TC, Dabisch PA, Garza NL, et al. A characterization of aerosolized Sudan virus infection in African green monkeys, cynomolgus macaques, and rhesus macaques. *Viruses.* 2012;4(10):2115-36.

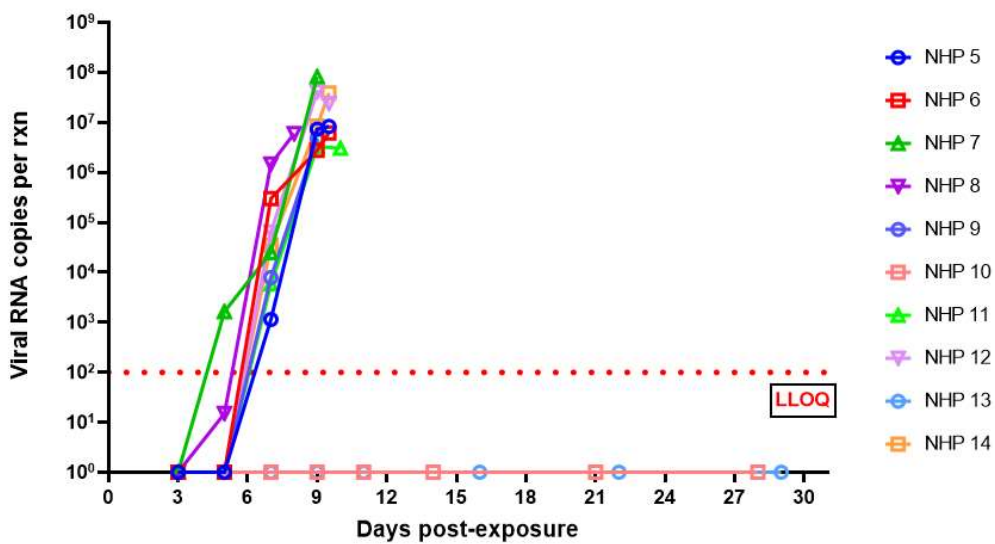
Appendices

Clinical Analysis

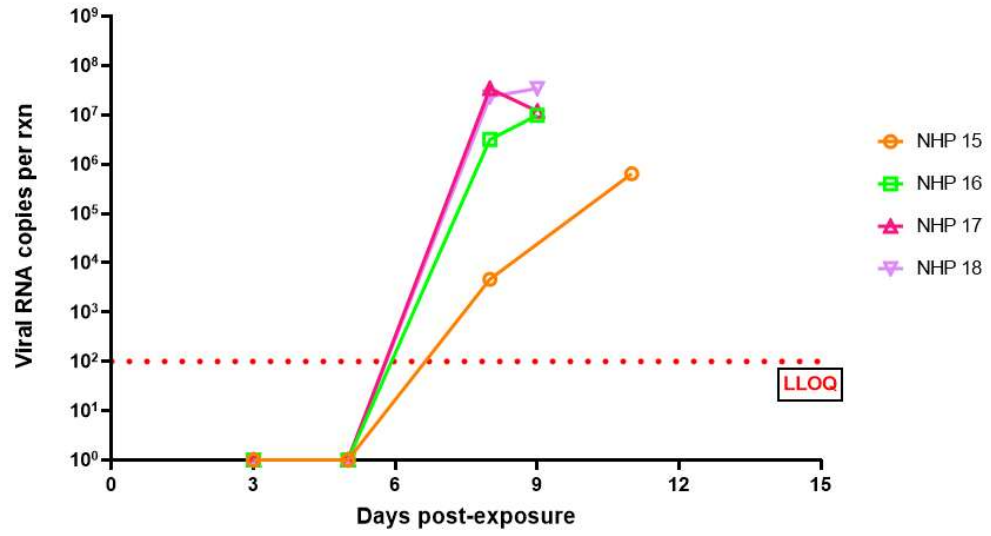
Plasma viral load by qRT-PCR
100 pfu



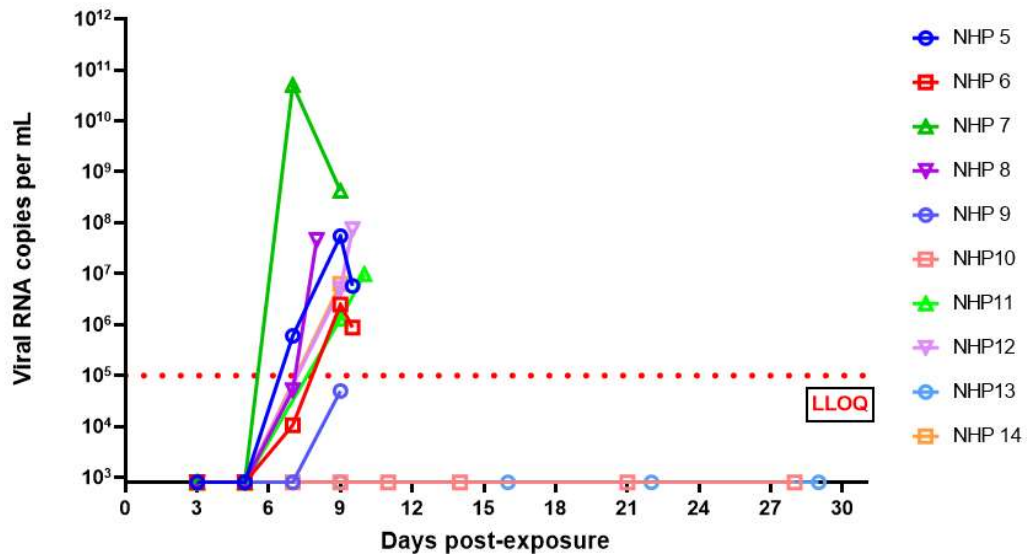
Plasma viral load by qRT-PCR
1000 pfu



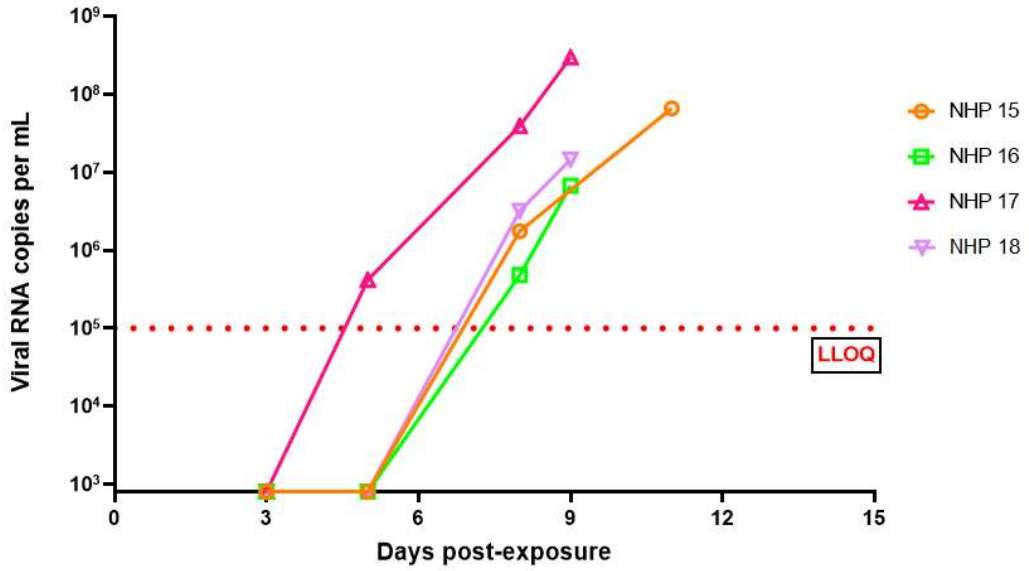
Plasma viral load by qRT-PCR
10000 pfu



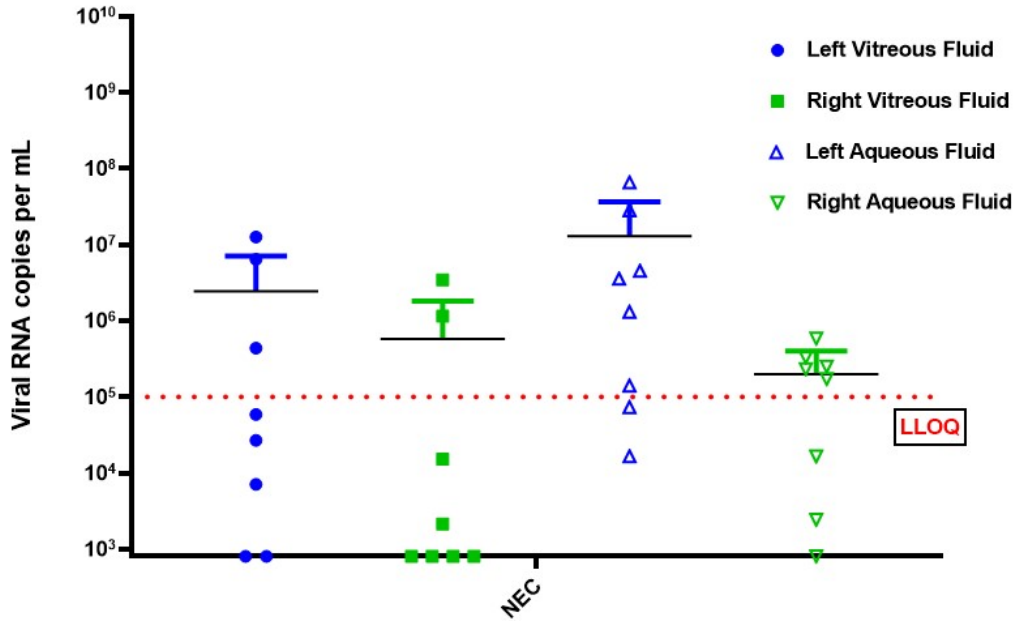
Nasal viral load by qRT-PCR
1000 pfu



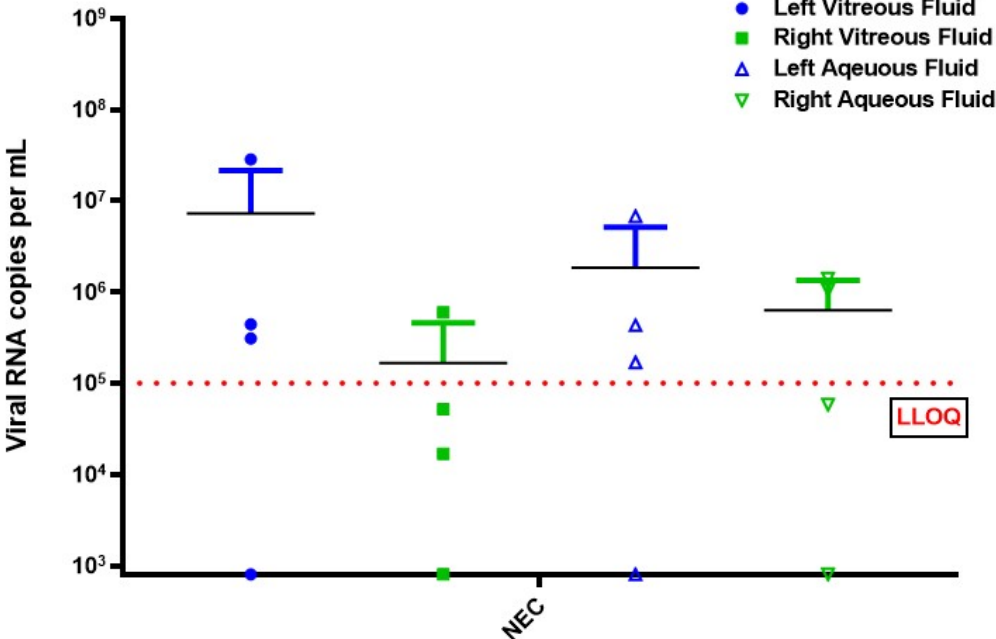
Nasal viral load by qRT-PCR
10000 pfu



Fluid viral load by qRT-PCR
1000 pfu

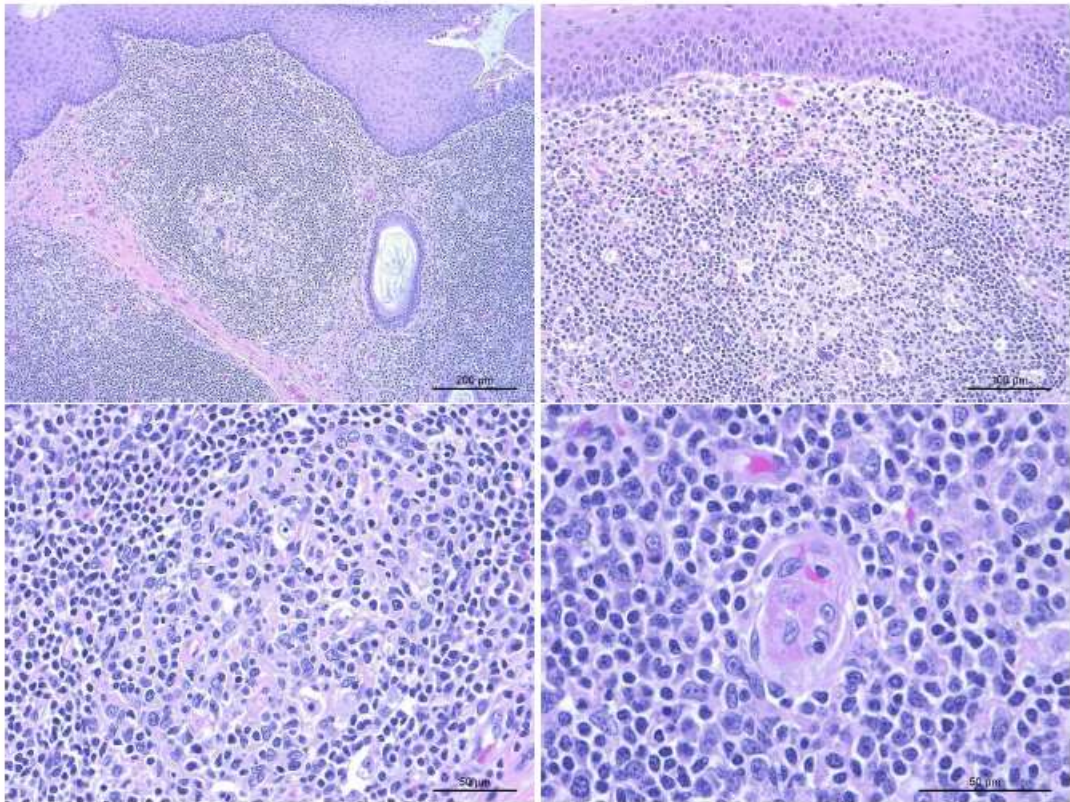


Fluid viral load by qRT-PCR
10000 pfu

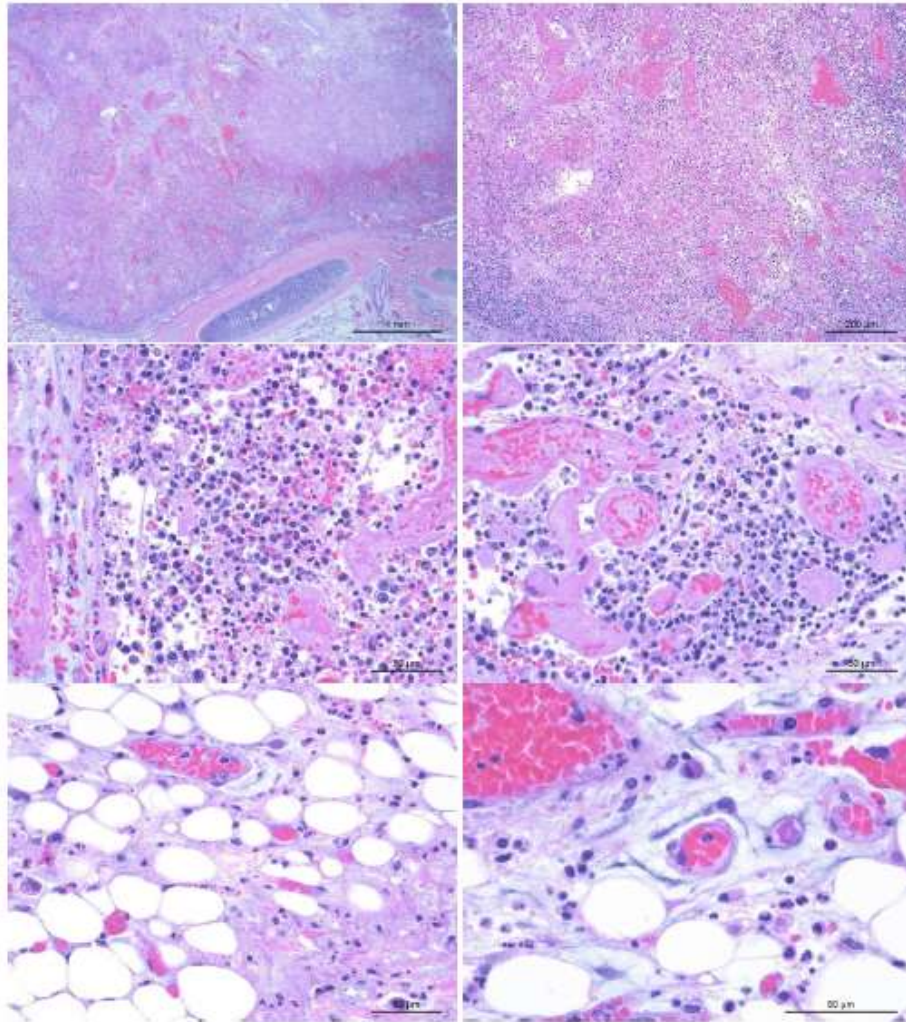


Pathology IHC

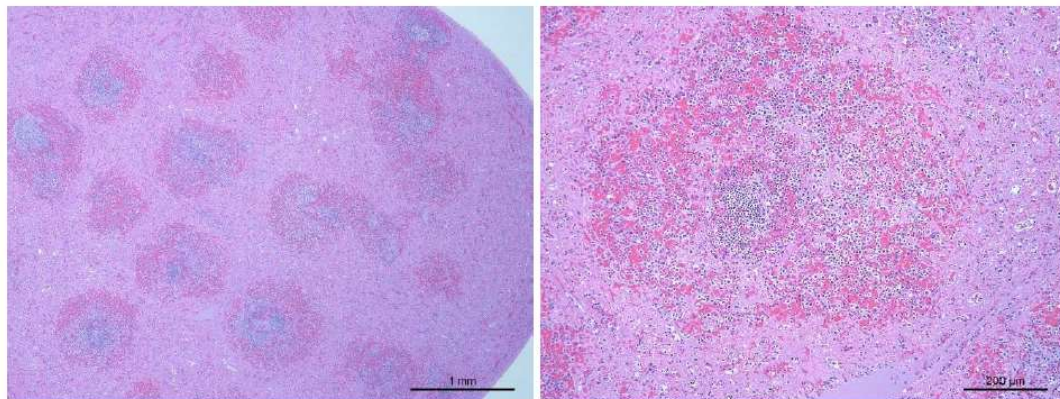
NHP 6 IHC staining of tonsils (1000 PFU)



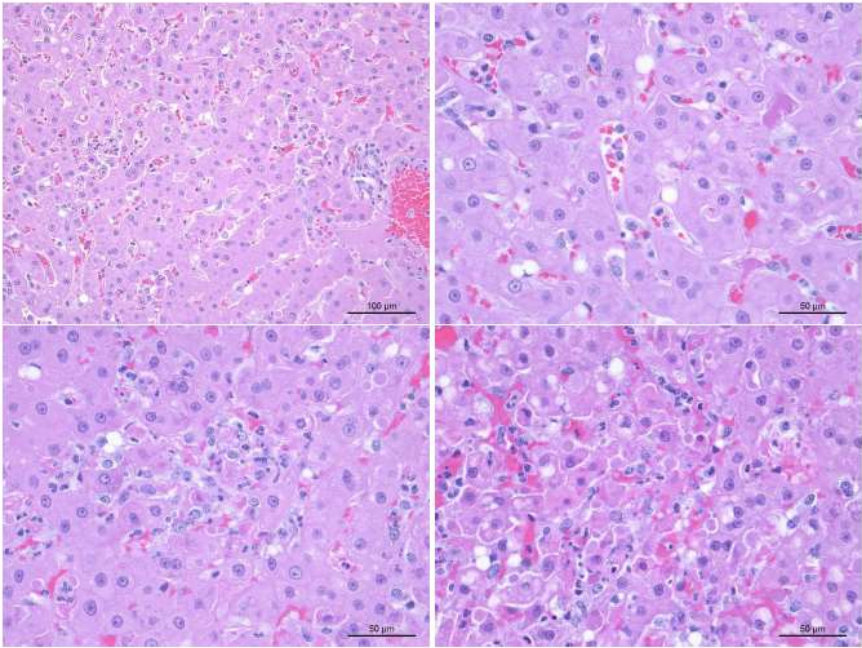
NHP 7 IHC staining of the trachea



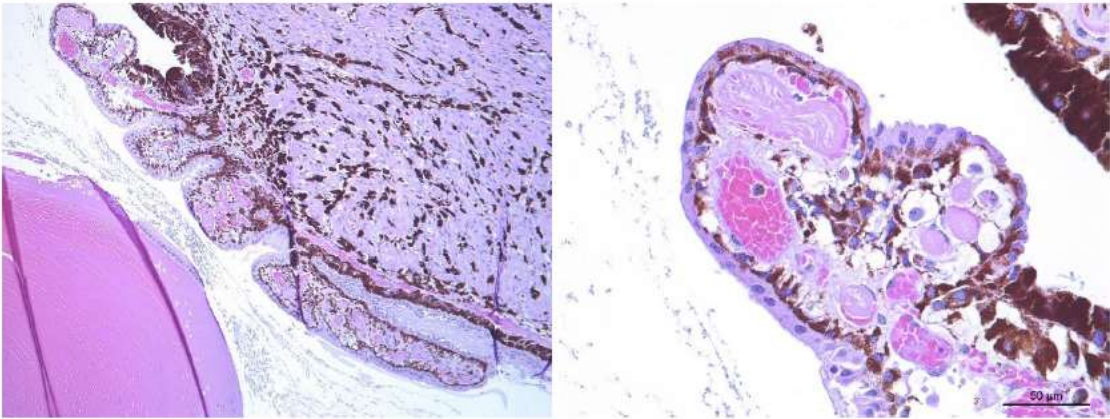
NHP 7 IHC staining of the spleen (1000 PFU)



NHP 8 IHC staining of the liver (1000 PFU)

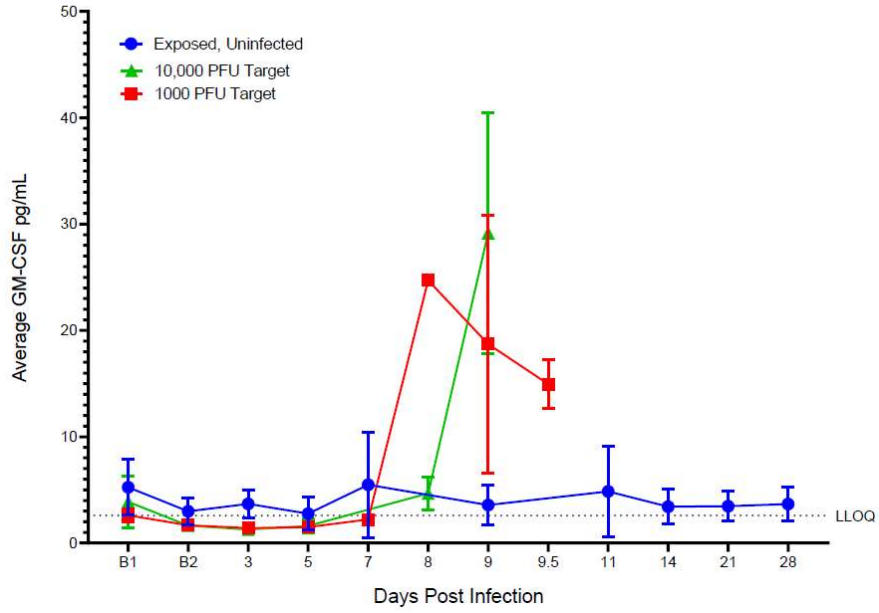


NHP 8 IHC staining of an ocular globe (1000 PFU)

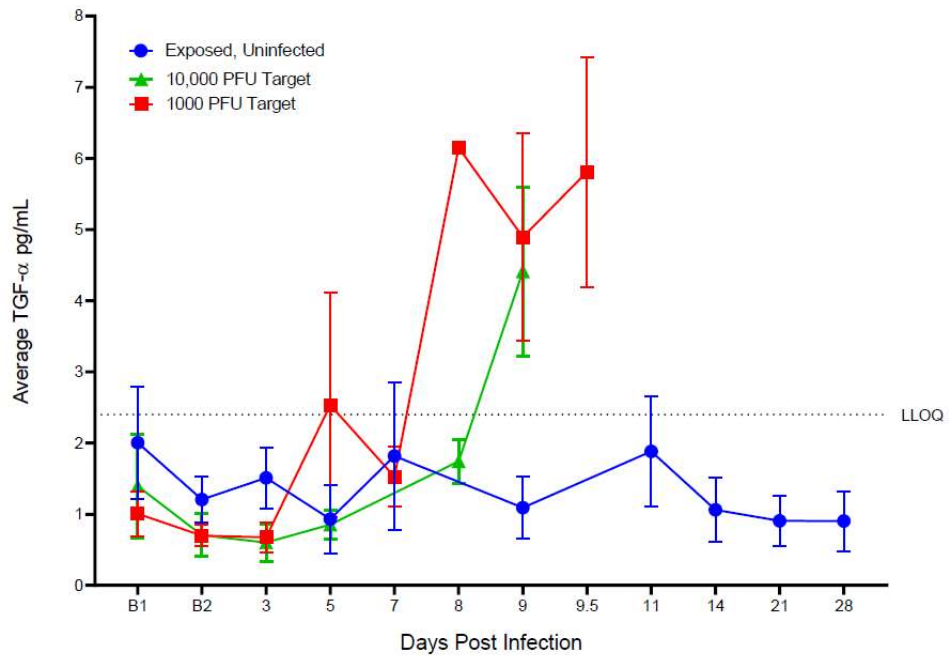


Cytokine Analysis

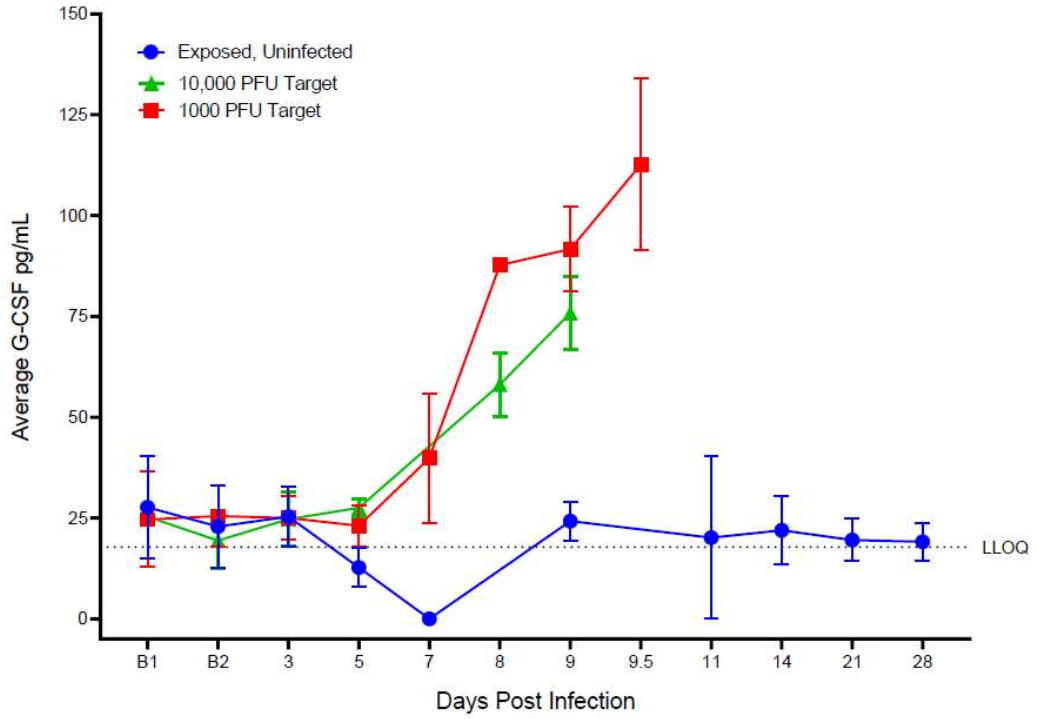
Non-Human Primate Cytokine/Chemokine 23-Plex



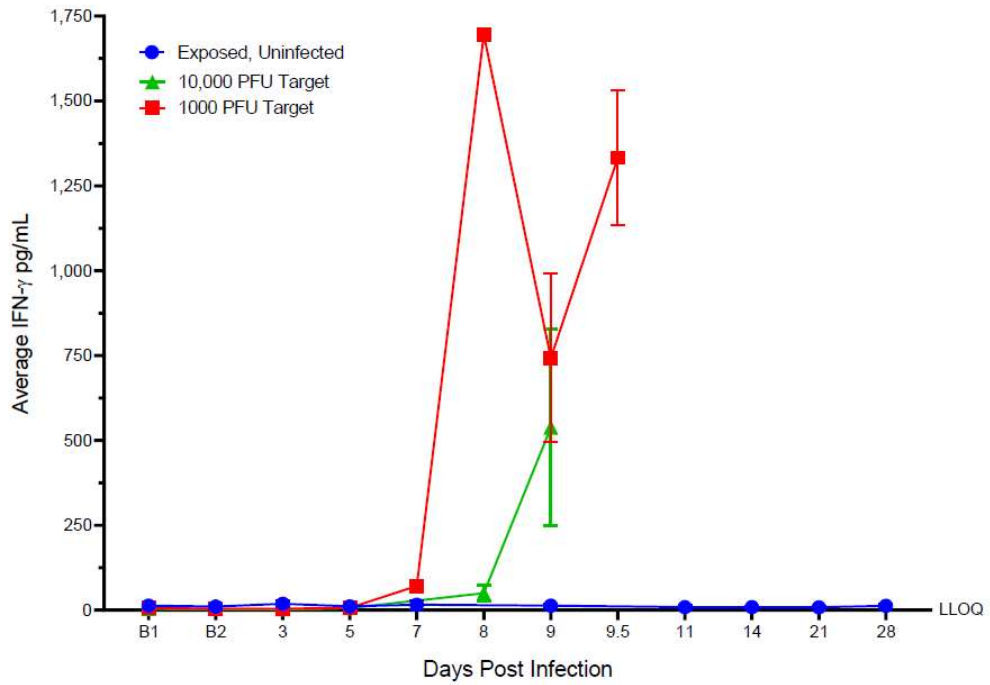
Non-Human Primate Cytokine/Chemokine 23-Plex



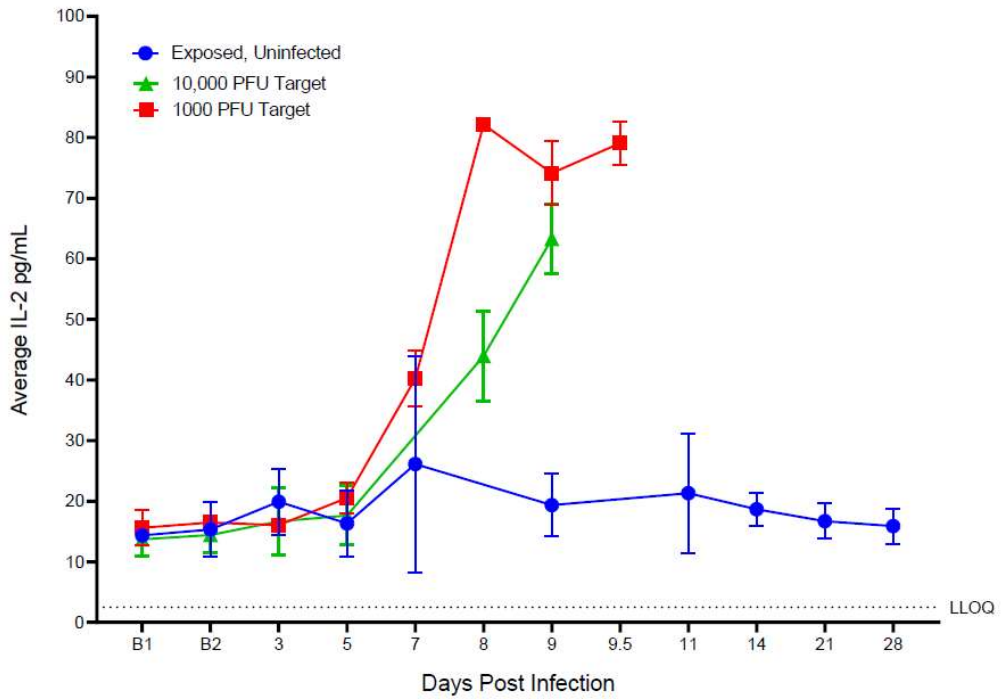
Non-Human Primate Cytokine/Chemokine 23-Plex



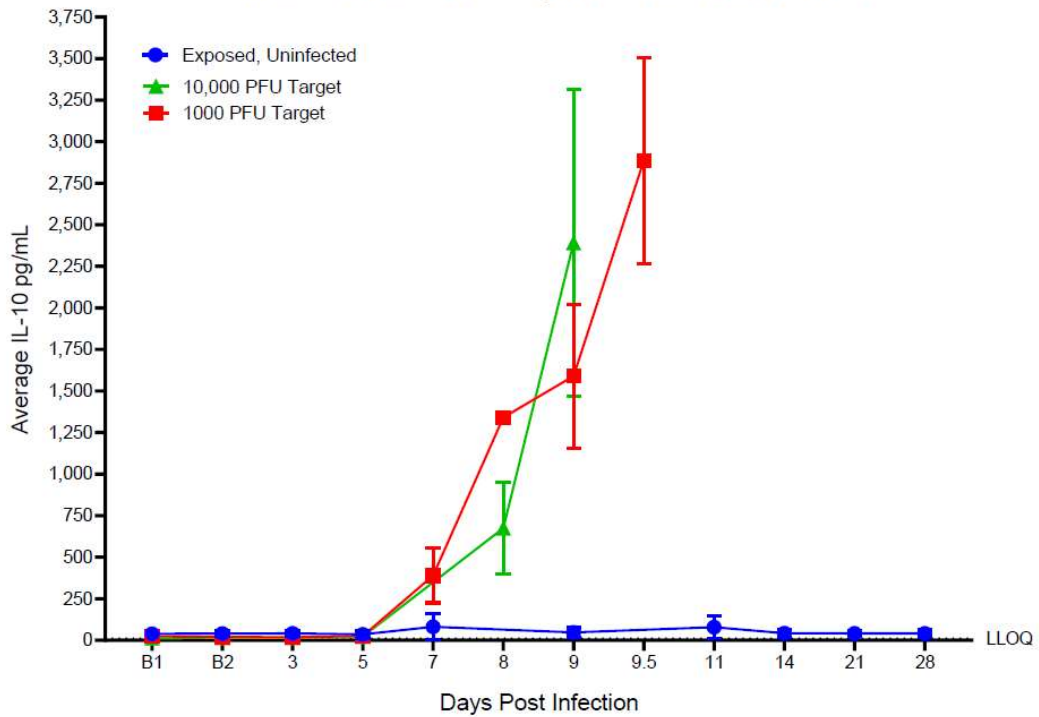
Non-Human Primate Cytokine/Chemokine 23-Plex



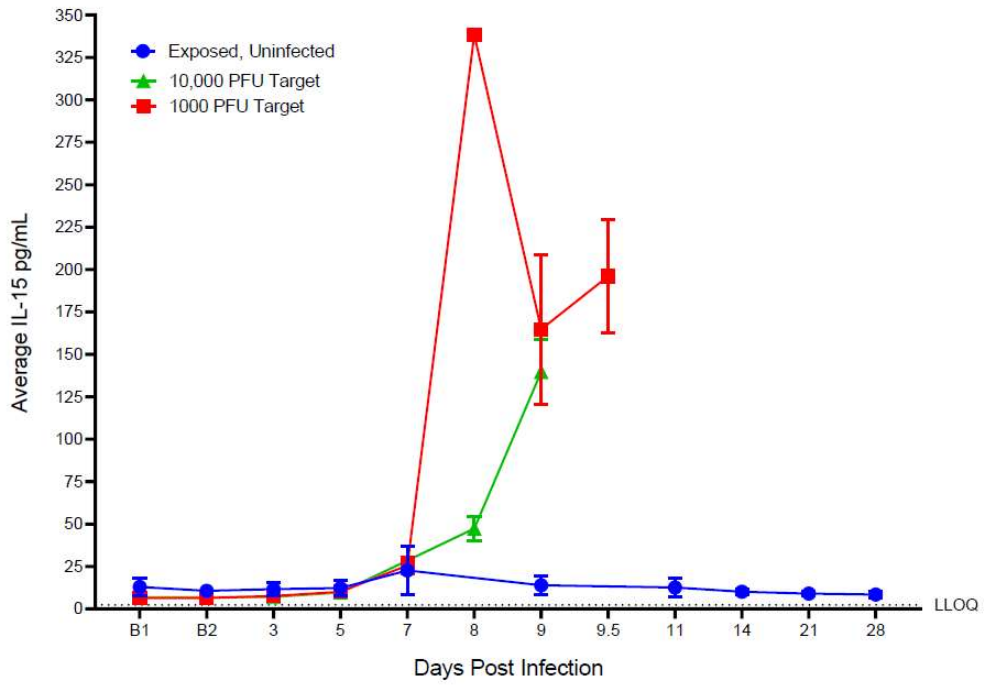
Non-Human Primate Cytokine/Chemokine 23-Plex



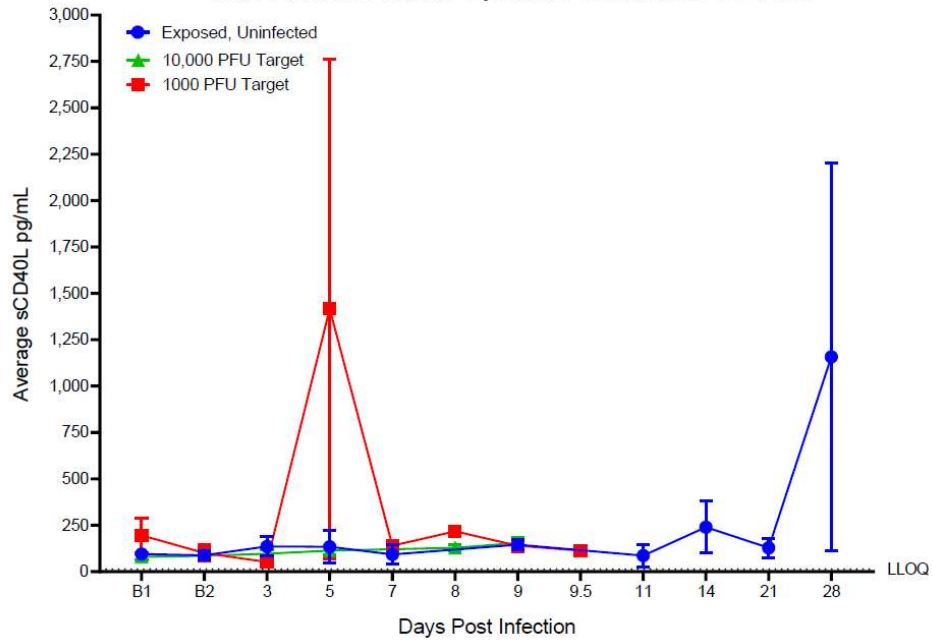
Non-Human Primate Cytokine/Chemokine 23-Plex



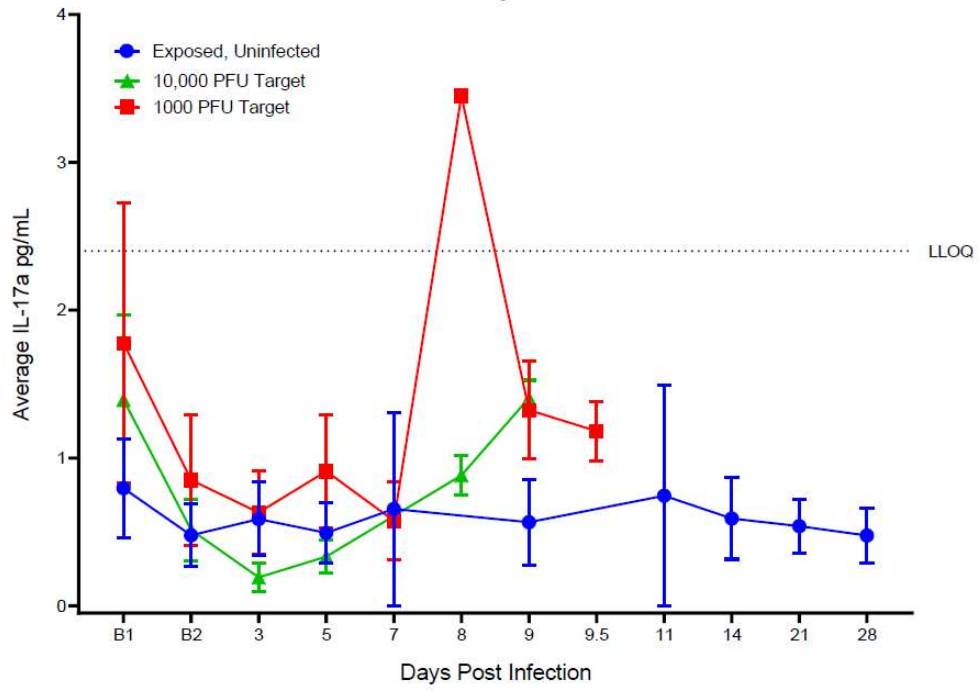
Non-Human Primate Cytokine/Chemokine 23-Plex



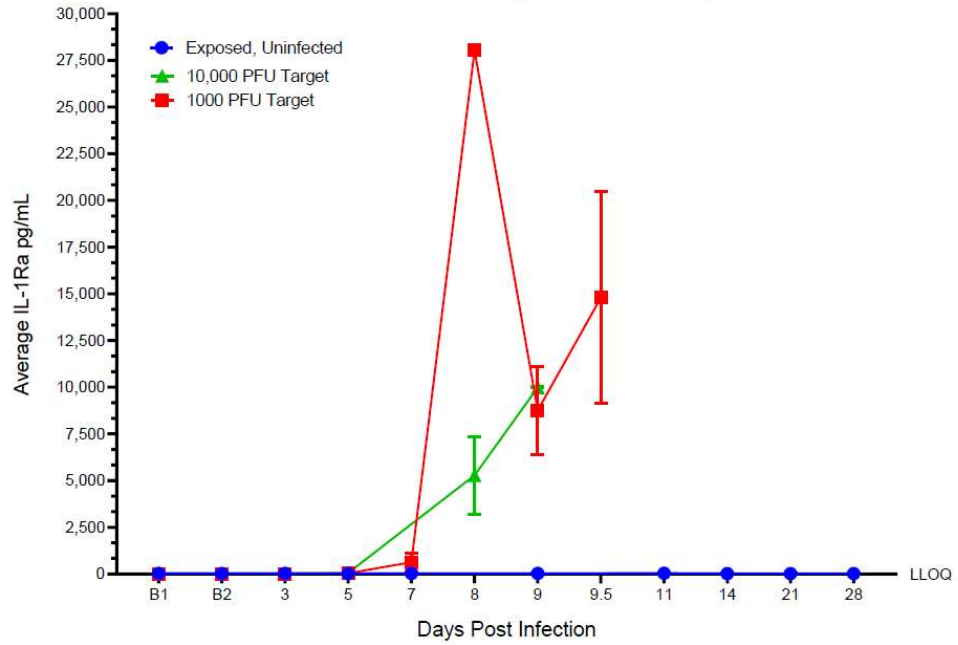
Non-Human Primate Cytokine/Chemokine 23-Plex

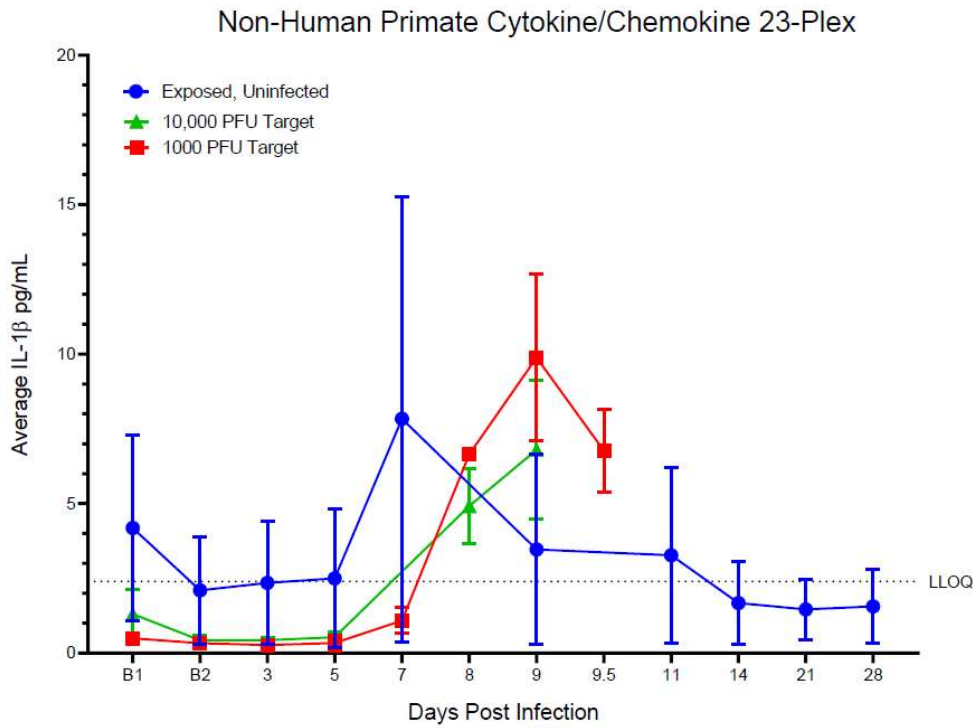
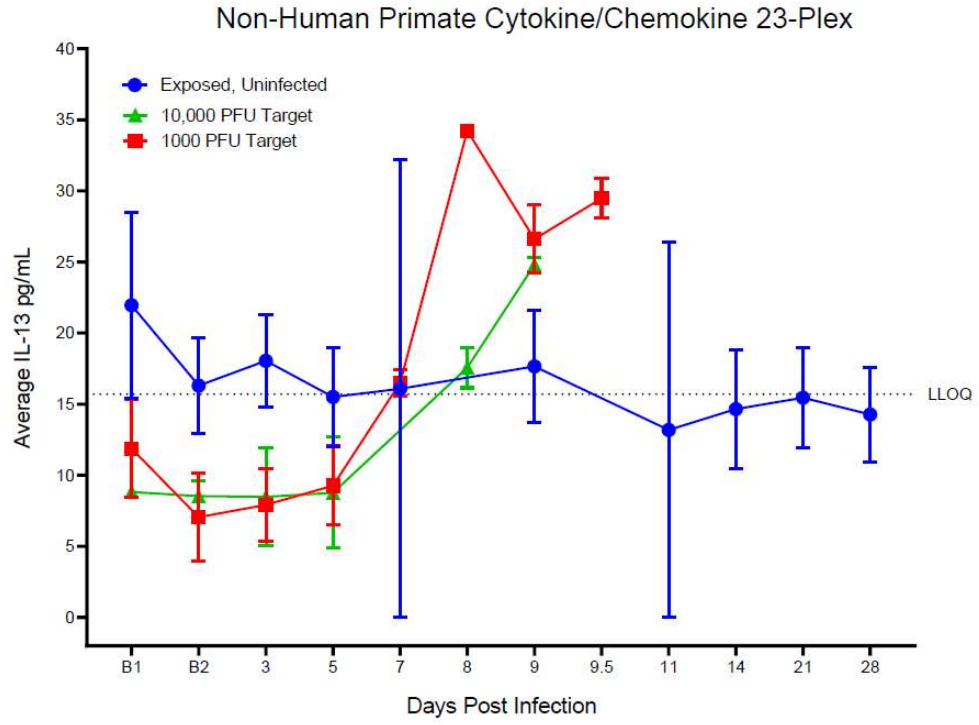


Non-Human Primate Cytokine/Chemokine 23-Plex

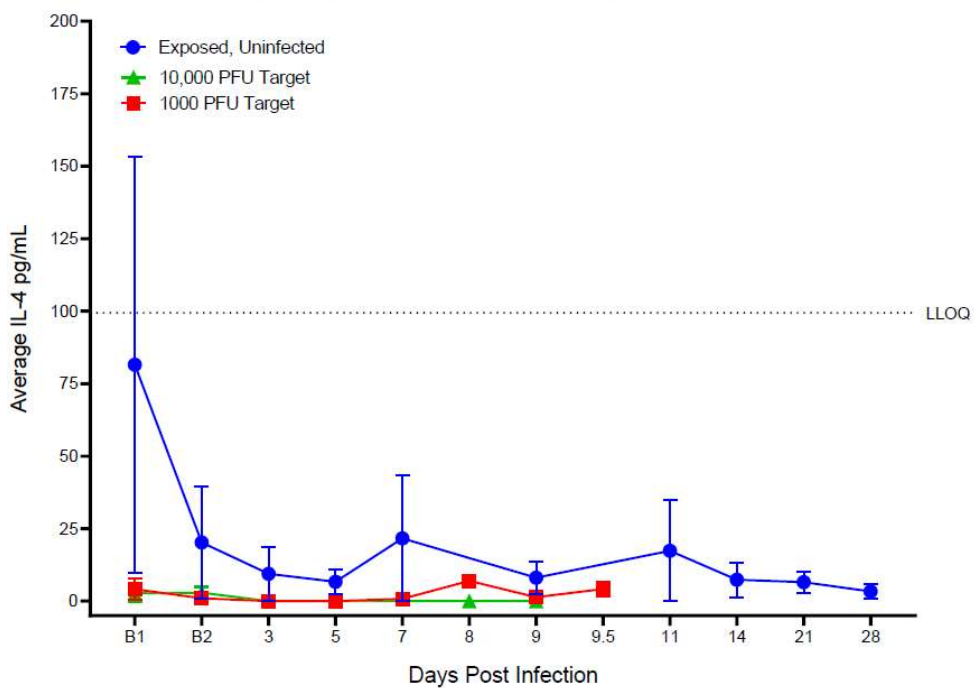


Non-Human Primate Cytokine/Chemokine 23-Plex

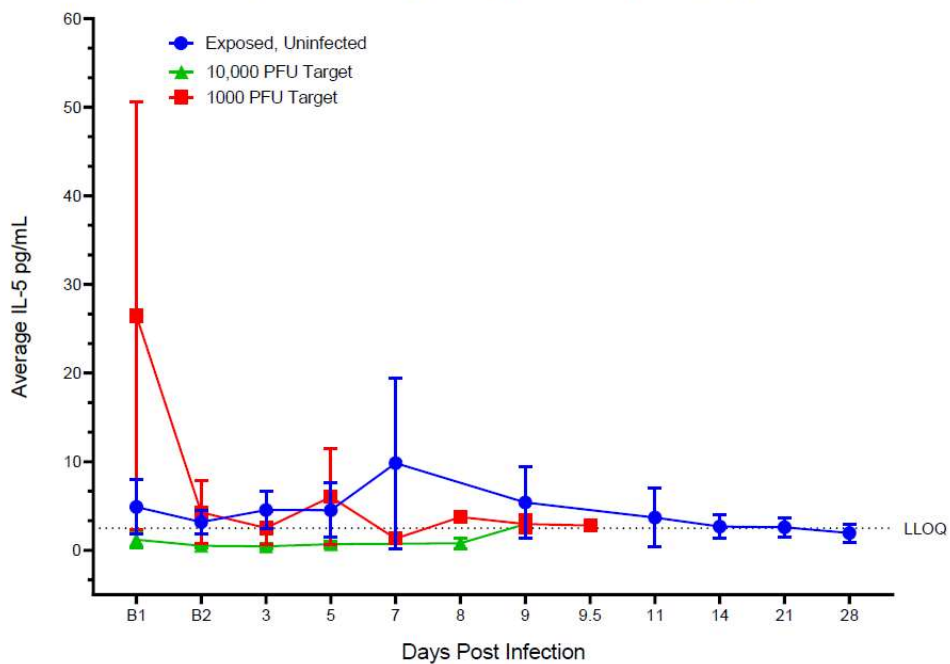




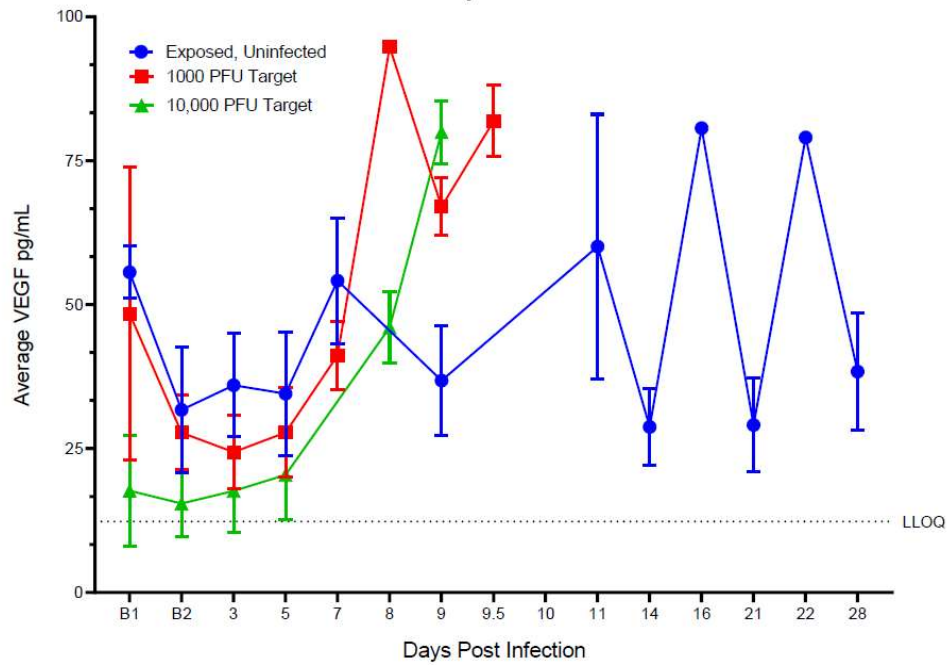
Non-Human Primate Cytokine/Chemokine 23-Plex



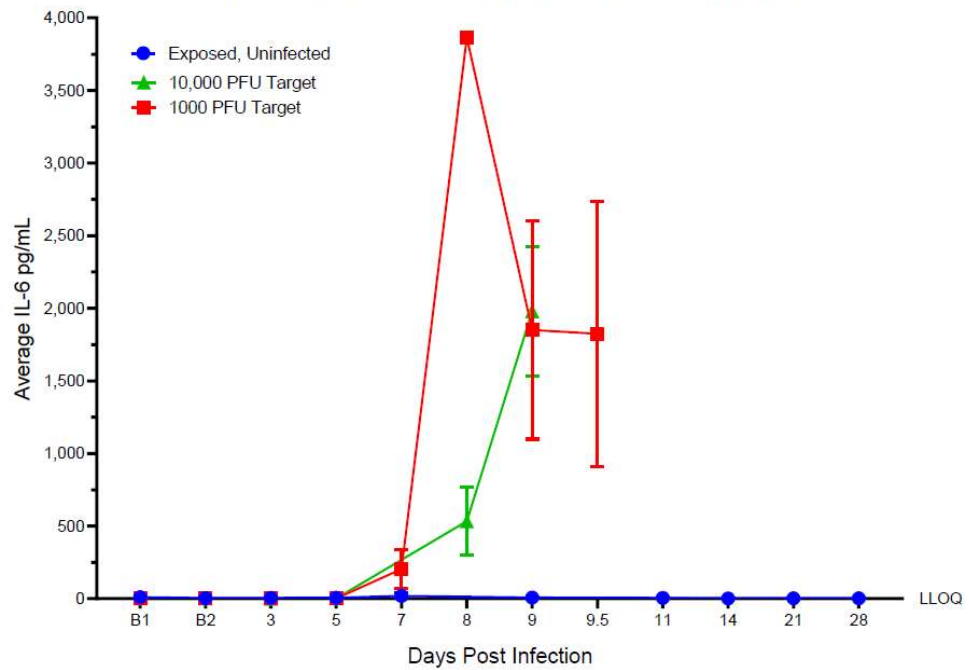
Non-Human Primate Cytokine/Chemokine 23-Plex



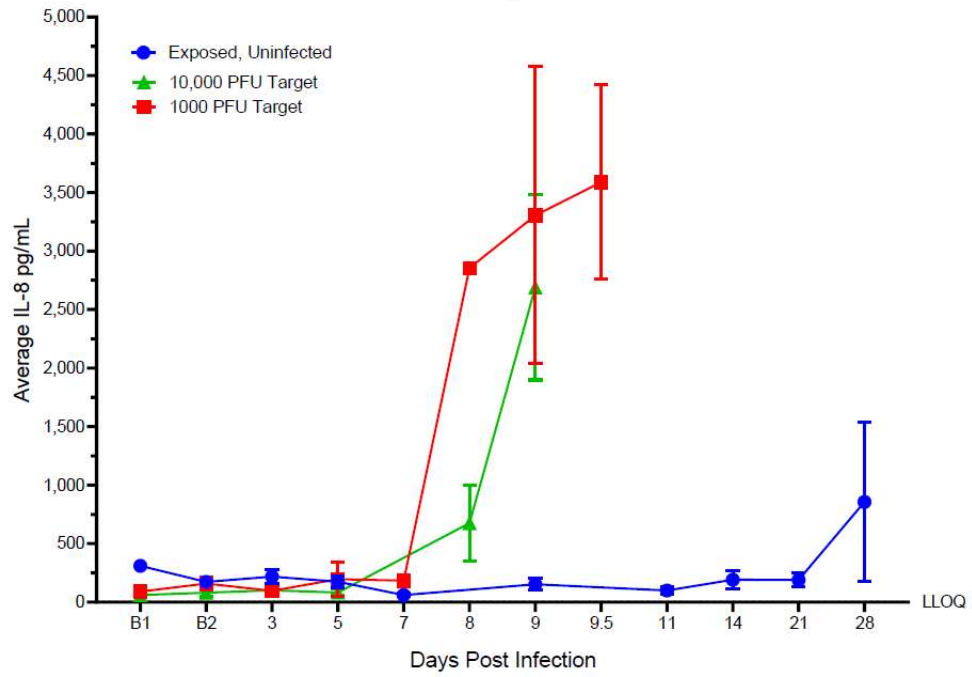
Non-Human Primate Cytokine/Chemokine 23-Plex



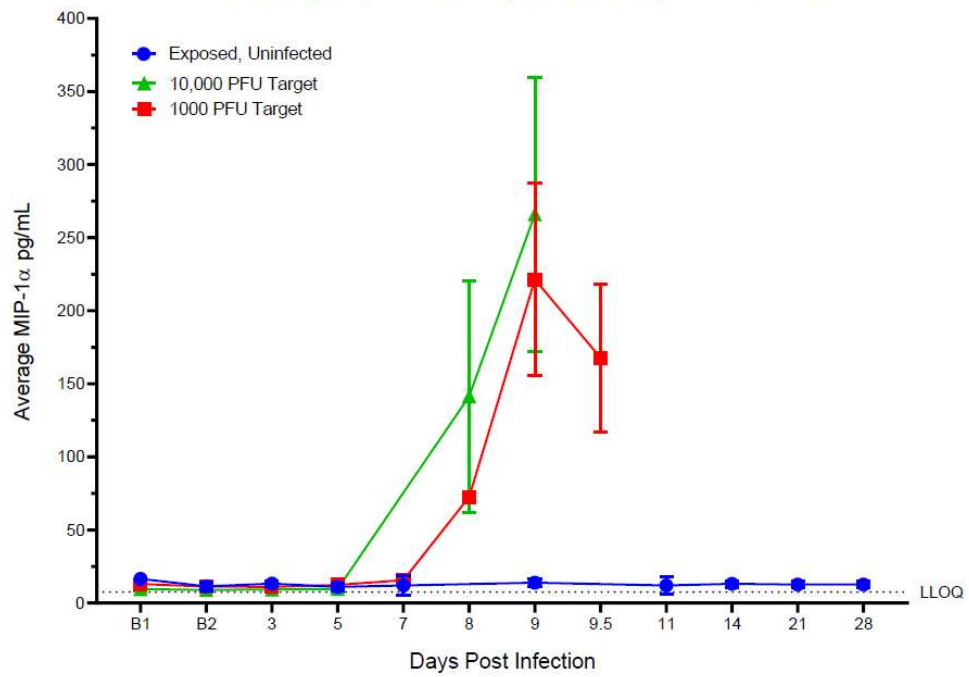
Non-Human Primate Cytokine/Chemokine 23-Plex



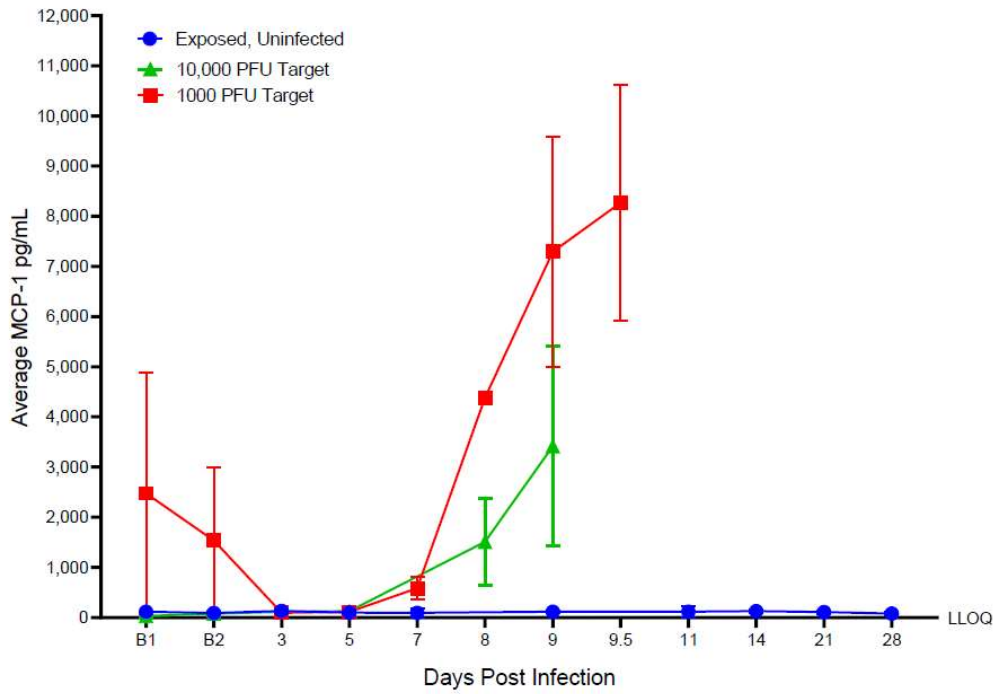
Non-Human Primate Cytokine/Chemokine 23-Plex



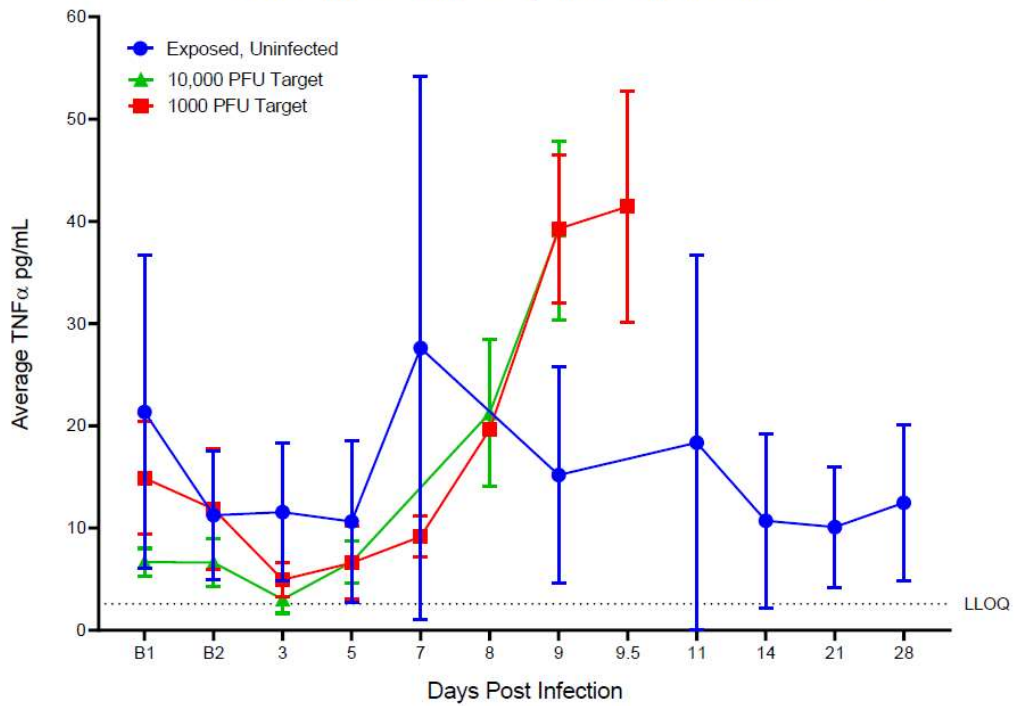
Non-Human Primate Cytokine/Chemokine 23-Plex

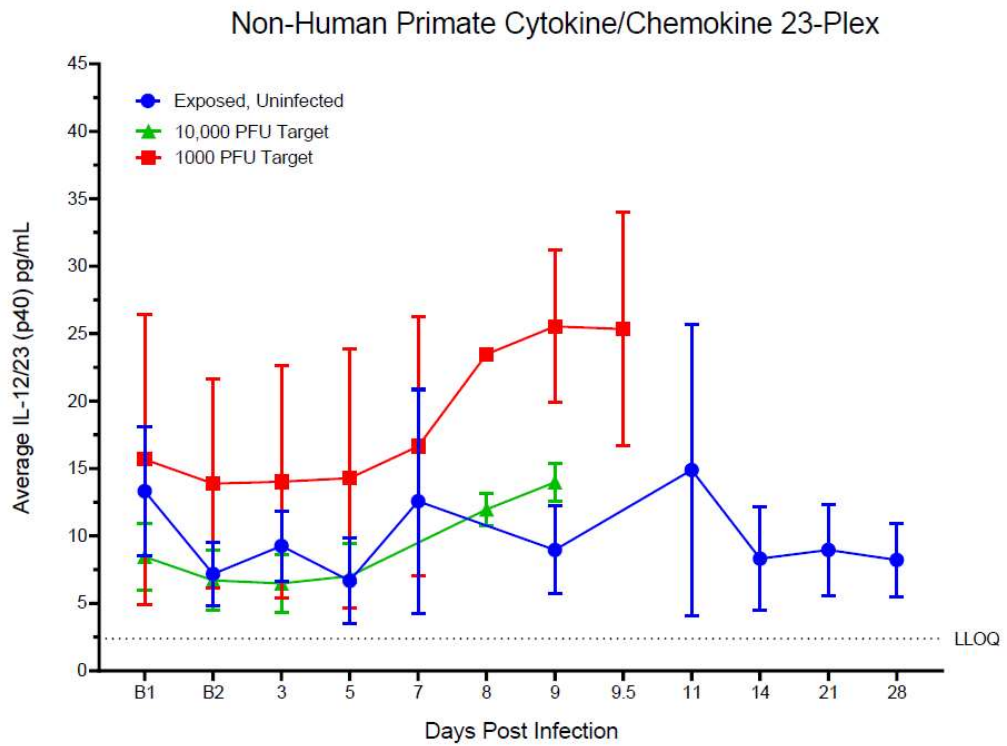
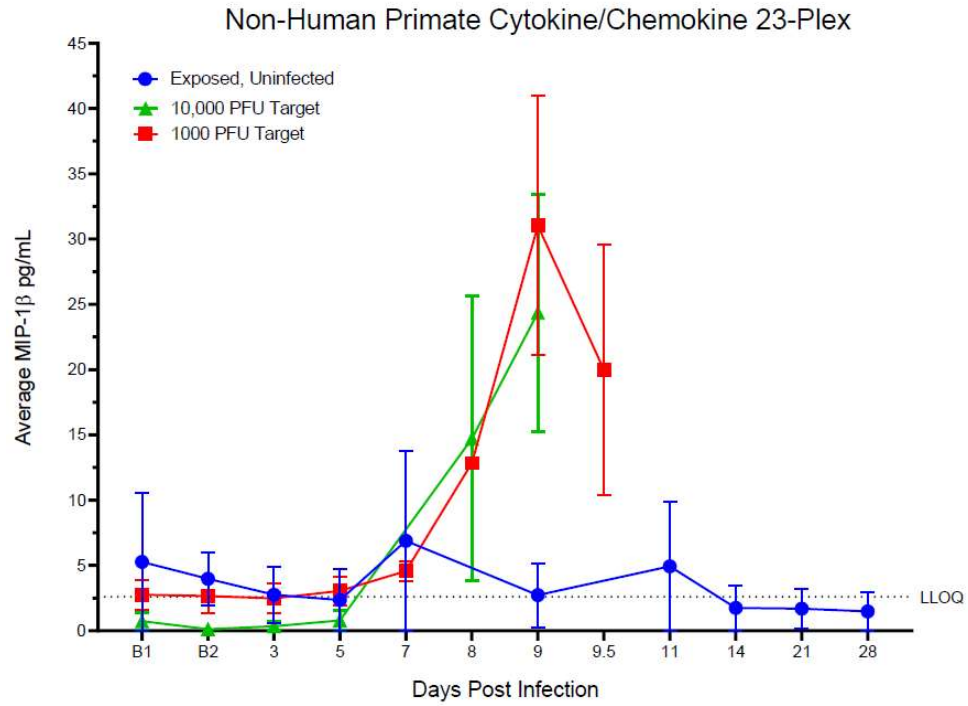


Non-Human Primate Cytokine/Chemokine 23-Plex

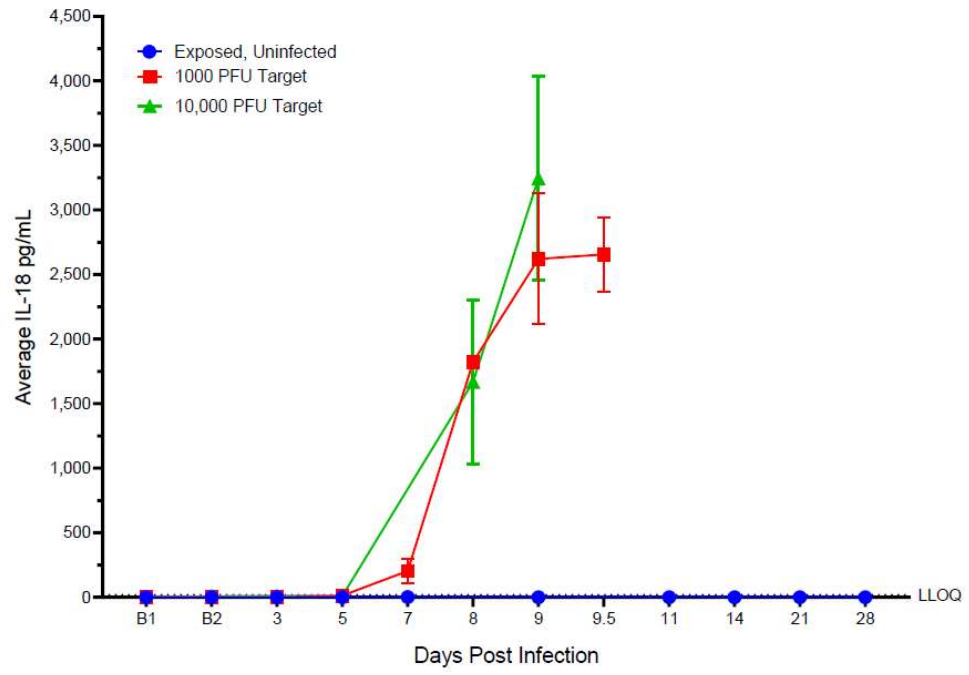


Non-Human Primate Cytokine/Chemokine 23-Plex



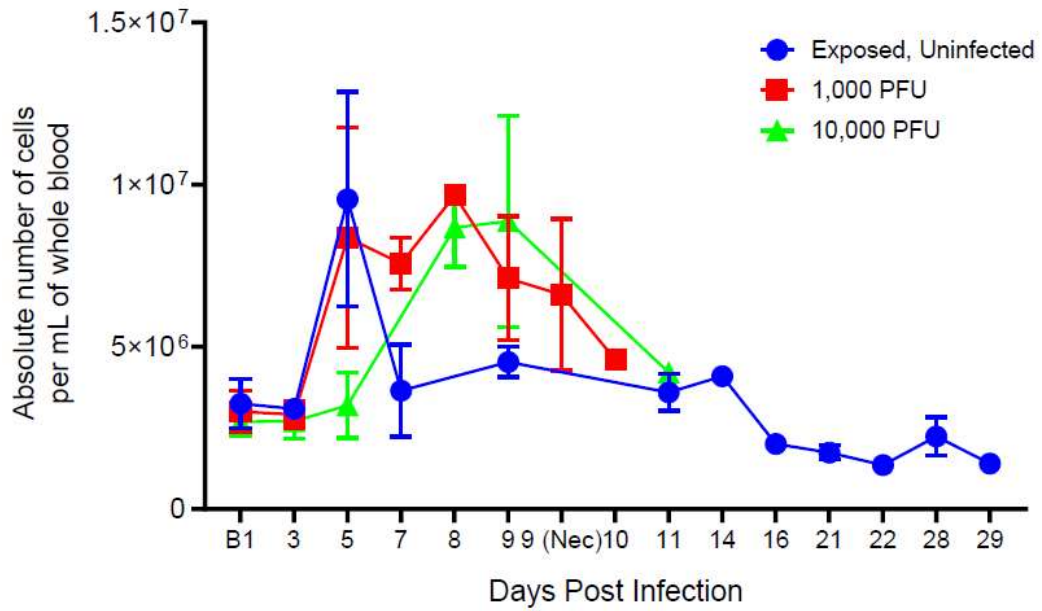


Non-Human Primate Cytokine/Chemokine 23-Plex

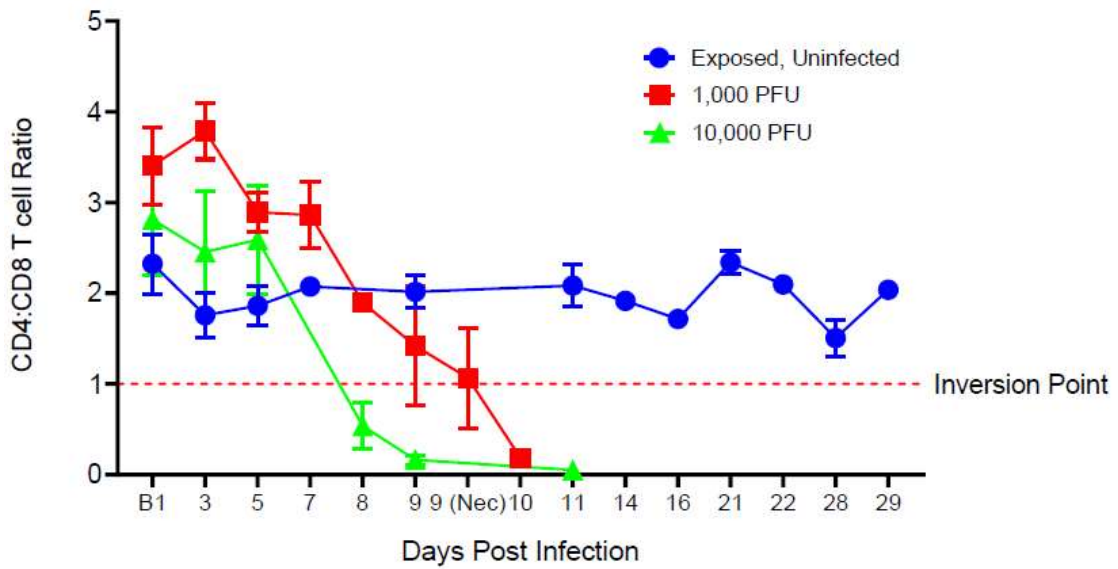


Flow Cytometry

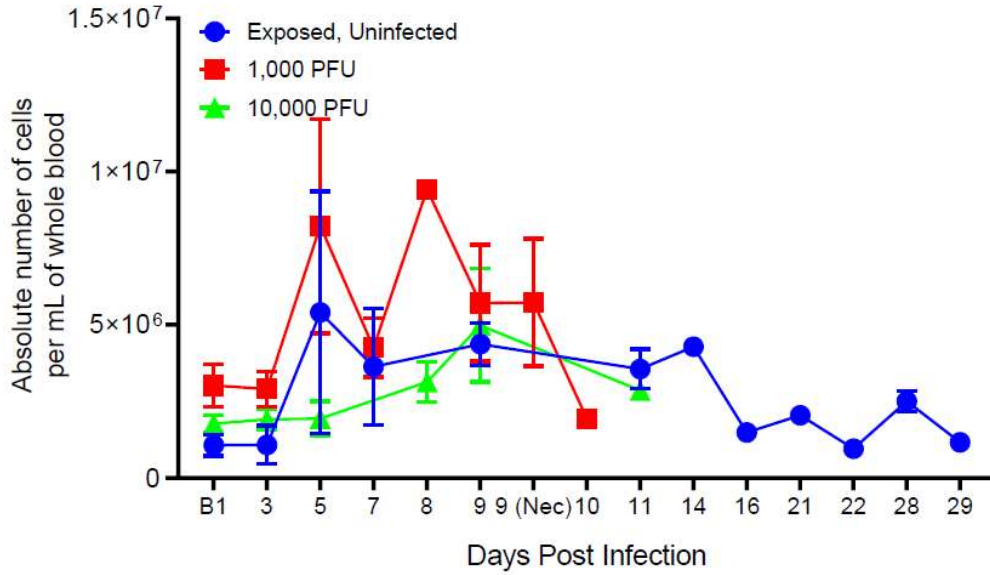
Total Granulocytes (CD20-, CD3-, NKG2a-, CD66+)



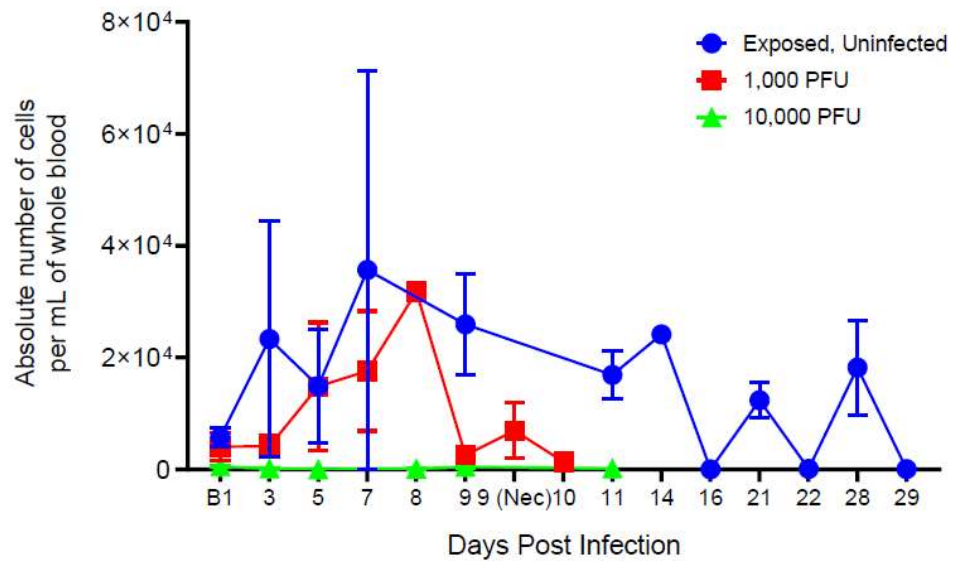
CD4:CD8 T cell Ratio



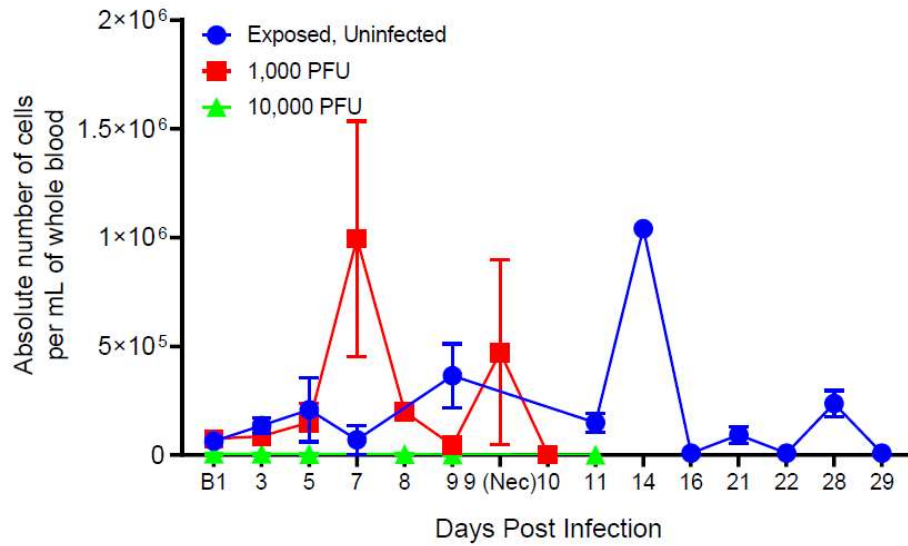
Total Monocytes (CD20-, CD3-, CD14+)



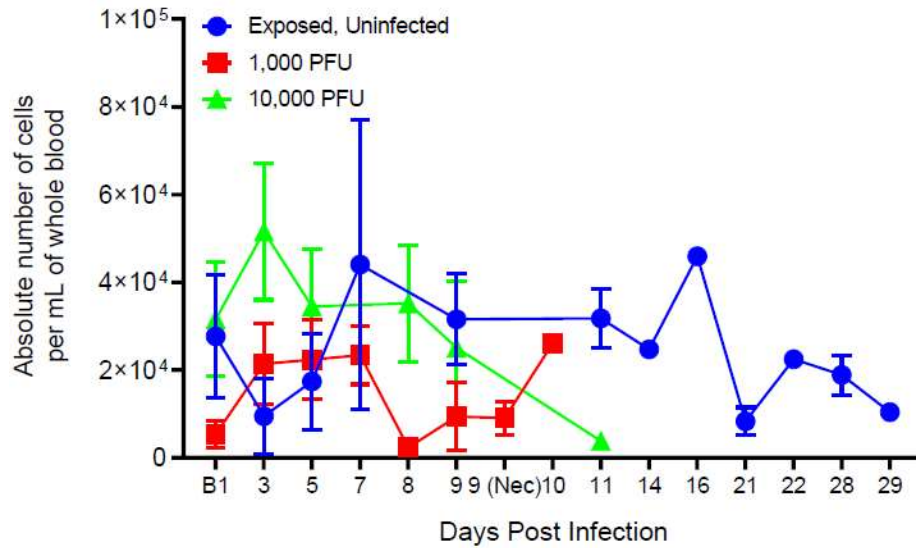
Intermediate Monocytes (CD20-, CD3-, CD14+, CD16+)



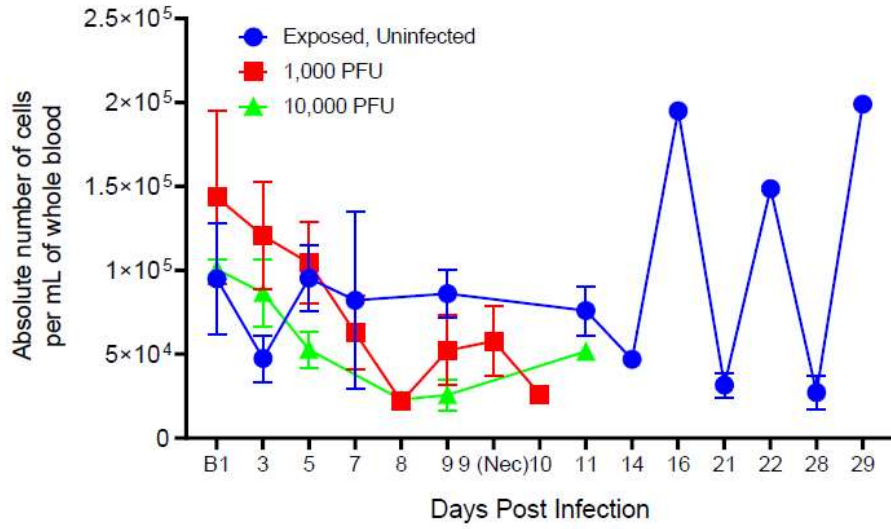
Macrophages (CD20-, CD3-, CD14-, HLA-DR+, CD163+)



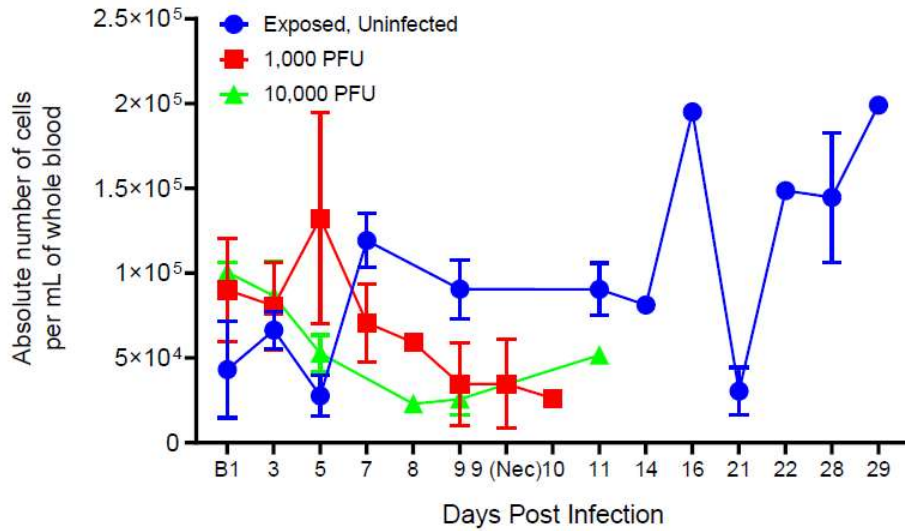
Myeloid Dendritic Cells (CD20-, CD3-, CD14-, HLA-DR+, CD11c+)

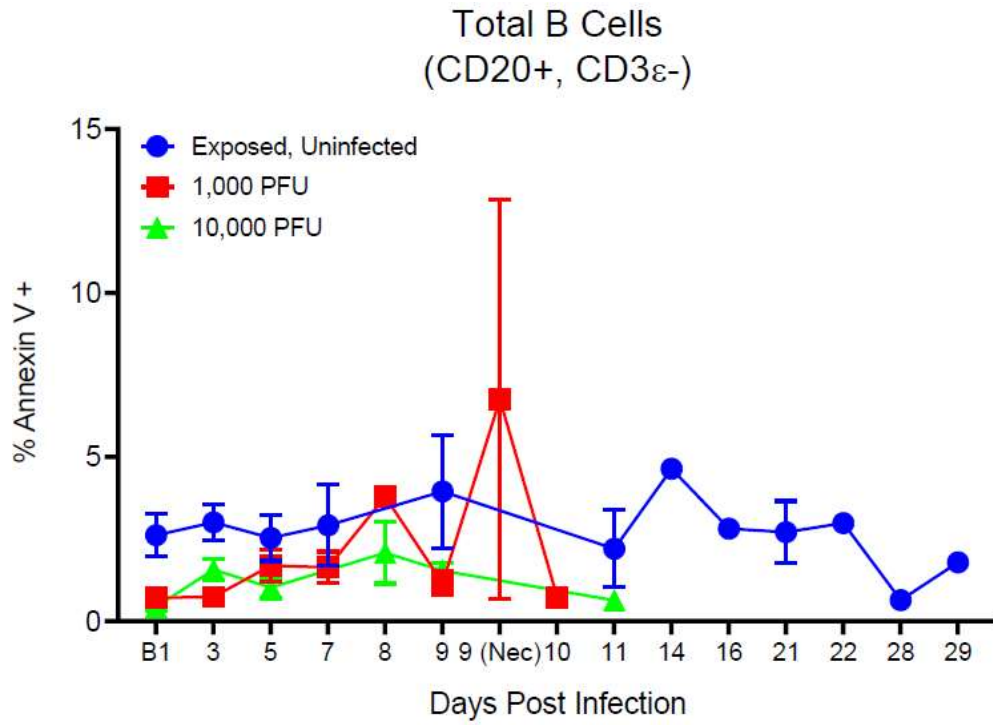
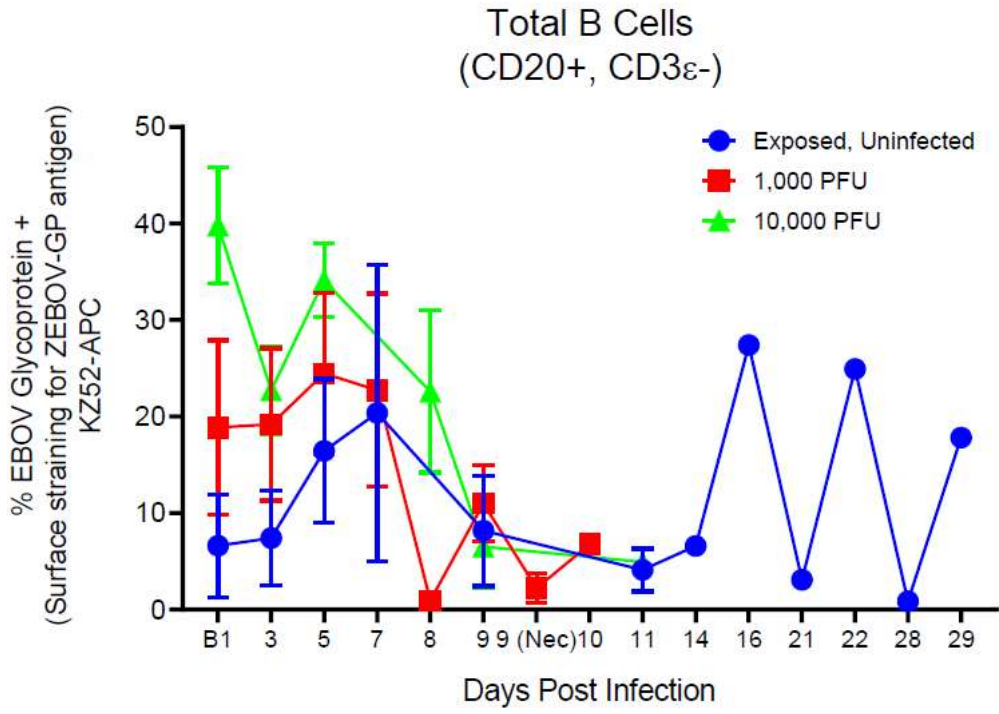


Inflammatory Natural Killer Cells
(CD20-, CD3-, CD14-, HLA-DR-, NKG2a+, CD8+, CD16-)

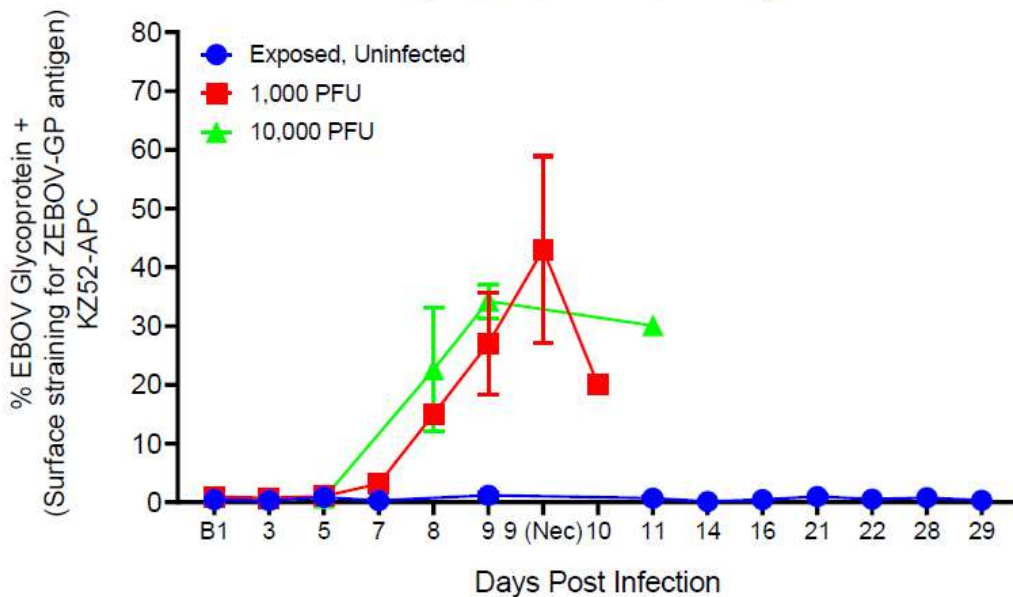


Cytolytic Natural Killer Cells
(CD20-, CD3-, CD14-, HLA-DR-, NKG2a+, CD8+, CD16+)

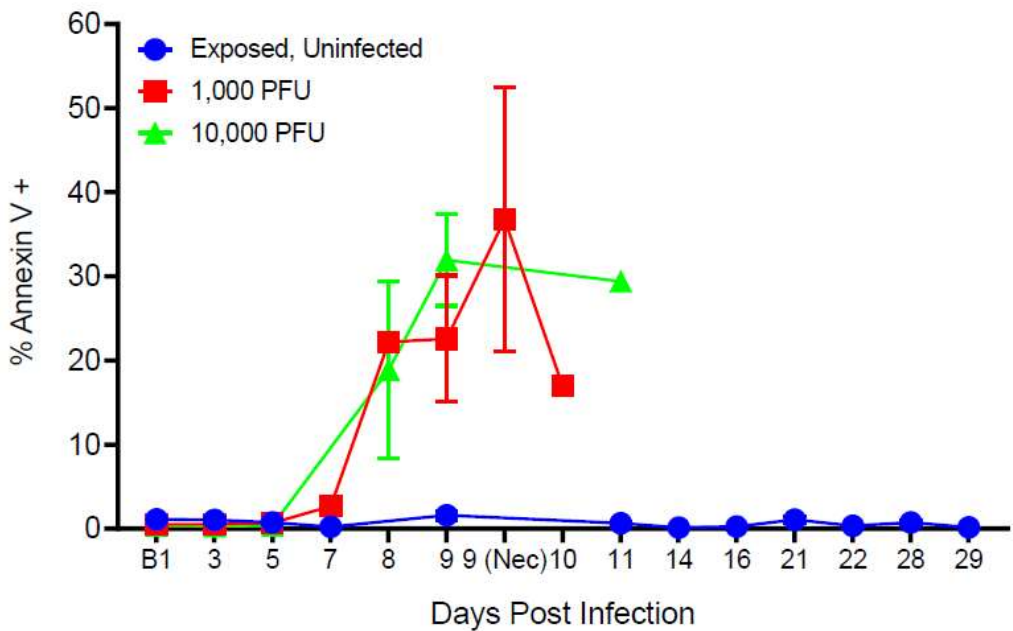




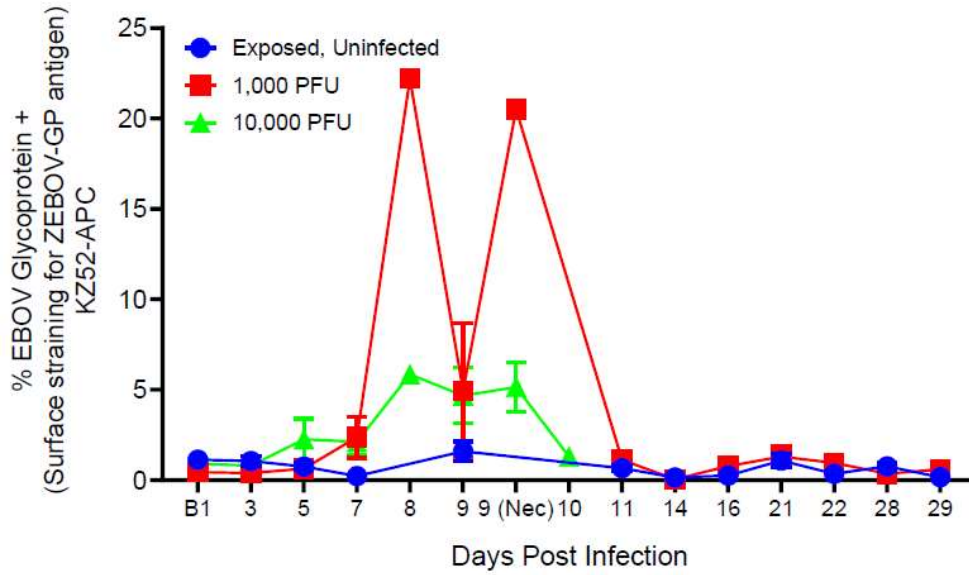
Total CD4 T Cells
(CD20-, CD3+, CD4+)



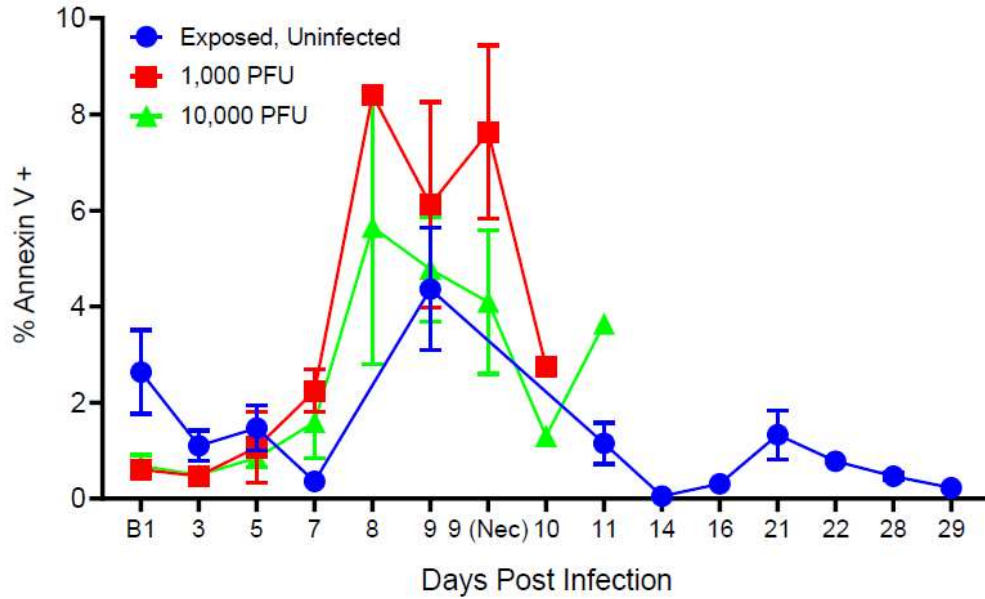
Total CD4 T Cells
(CD20-, CD3+, CD4+)



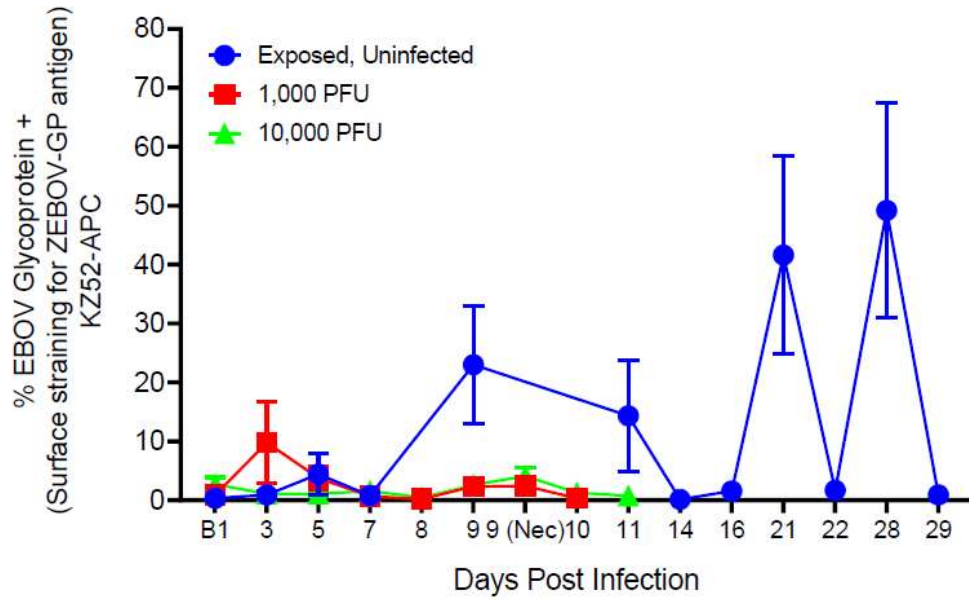
Total CD8 T Cells
(CD20-, CD3+, CD8+)



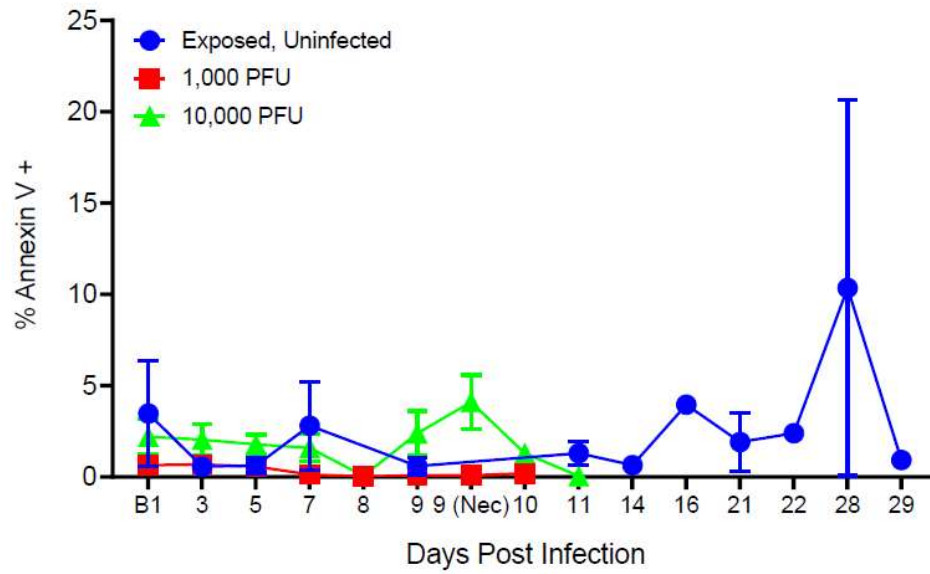
Total CD8 T Cells
(CD20-, CD3+, CD8+)



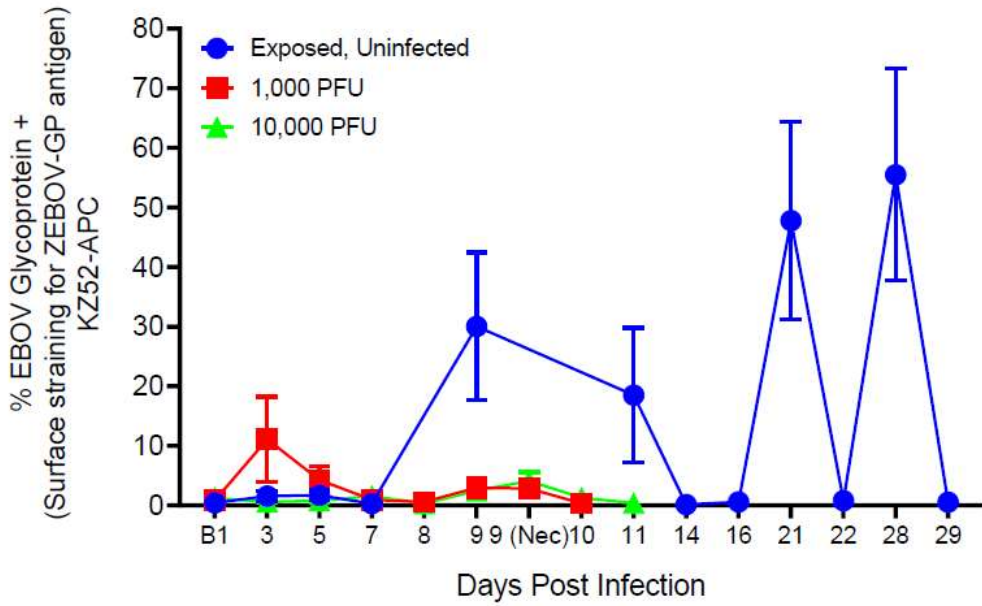
Total Granulocytes
(CD20-, CD3-, NKG2a-, CD66+)



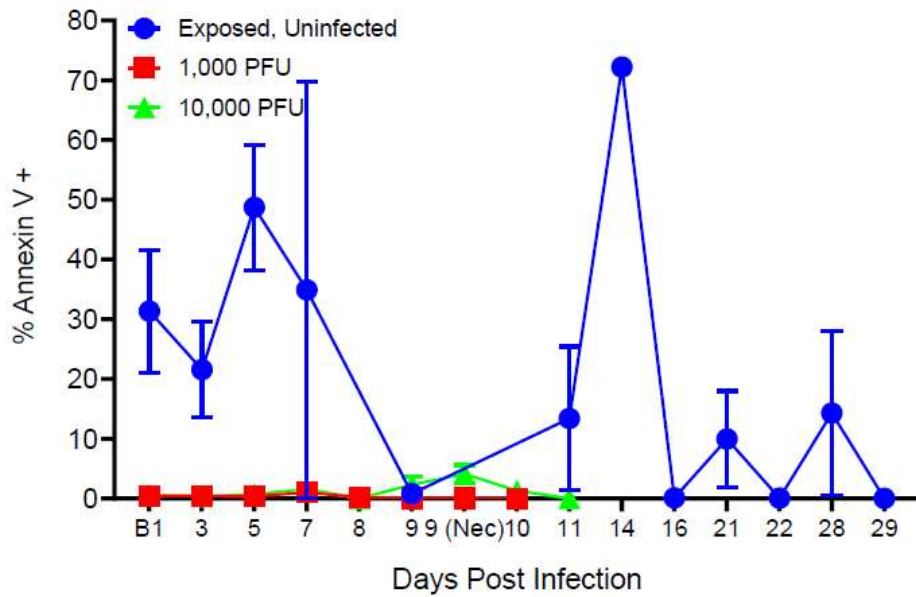
Total Granulocytes
(CD20-, CD3-, NKG2a-, CD66+)

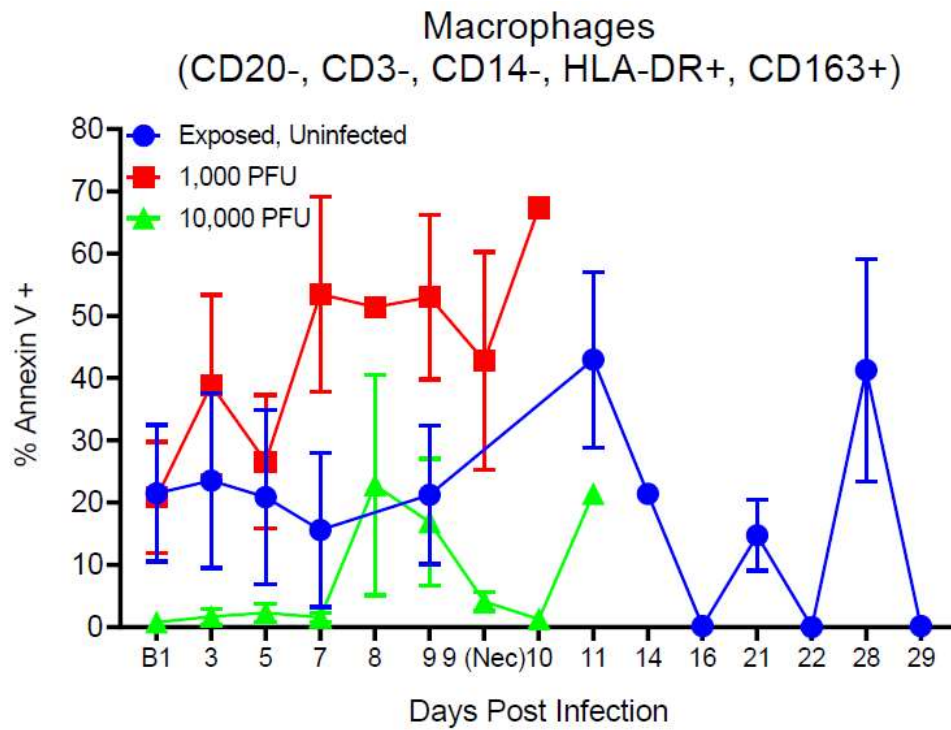
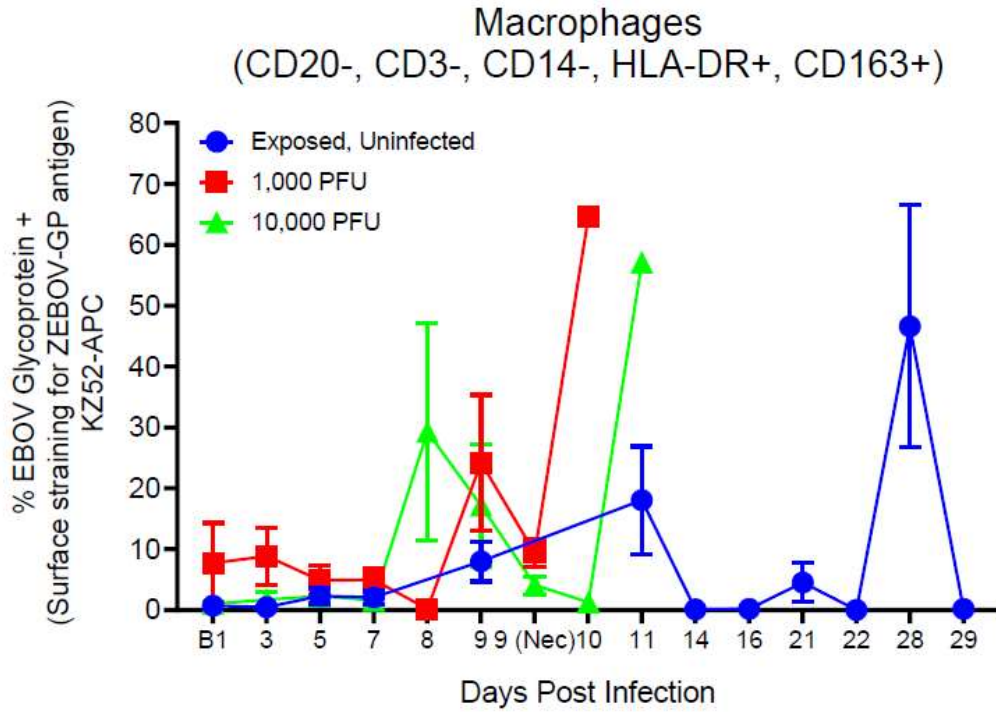


Total Monocytes (CD20-, CD3-, CD14+)

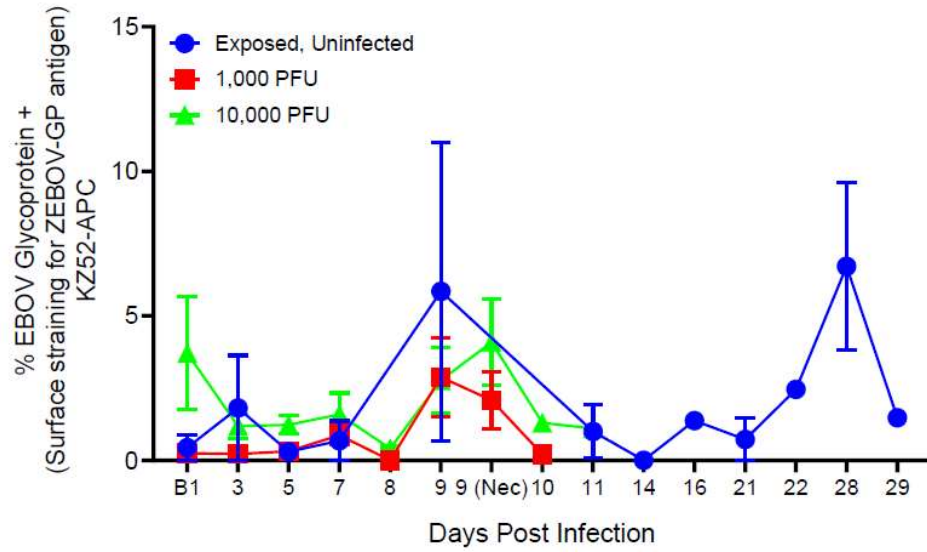


Total Monocytes (CD20-, CD3-, CD14+)





Myeloid Dendritic Cells
(CD20-, CD3-, CD14-, HLA-DR+, CD11c+)



Myeloid Dendritic Cells
(CD20-, CD3-, CD14-, HLA-DR+, CD11c+)

